CO_2-induced ion and fluid transport in human retinal pigment epithelium

Jeffrey Adijanto,[1,2] Tina Banzon,[2] Stephen Jalickee,[2] Nam S. Wang,[1] and Sheldon S. Miller[2]

[1]Department of Chemical and Biomolecular Engineering, The University of Maryland, College Park, MD 20742
[2]National Institutes of Health, National Eye Institute, Bethesda, MD 20892

In the intact eye, the transition from light to dark alters pH, $[Ca^{2+}]$, and [K] in the subretinal space (SRS) separating the photoreceptor outer segments and the apical membrane of the retinal pigment epithelium (RPE). In addition to these changes, oxygen consumption in the retina increases with a concomitant release of CO_2 and H_2O into the SRS. The RPE maintains SRS pH and volume homeostasis by transporting these metabolic byproducts to the choroidal blood supply. In vitro, we mimicked the transition from light to dark by increasing apical bath CO_2 from 5 to 13%; this maneuver decreased cell pH from 7.37 ± 0.05 to 7.14 ± 0.06 (n = 13). Our analysis of native and cultured fetal human RPE shows that the apical membrane is significantly more permeable (≈10-fold; n = 7) to CO_2 than the basolateral membrane, perhaps due to its larger exposed surface area. The limited CO_2 diffusion at the basolateral membrane promotes carbonic anhydrase–mediated HCO_3 transport by a basolateral membrane Na/$nHCO_3$ cotransporter. The activity of this transporter was increased by elevating apical bath CO_2 and was reduced by dorzolamide. Increasing apical bath CO_2 also increased intracellular Na from 15.7 ± 3.3 to 24.0 ± 5.3 mM (n = 6; $P < 0.05$) by increasing apical membrane Na uptake. The CO_2-induced acidification also inhibited the basolateral membrane Cl/HCO_3 exchanger and increased net steady-state fluid absorption from 2.8 ± 1.6 to 6.7 ± 2.3 μl × cm^{-2} × hr^{-1} (n = 5; $P < 0.05$). The present experiments show how the RPE can accommodate the increased retinal production of CO_2 and H_2O in the dark, thus preventing acidosis in the SRS. This homeostatic process would preserve the close anatomical relationship between photoreceptor outer segments and RPE in the dark and light, thus protecting the health of the photoreceptors.

The Journal of General Physiology

INTRODUCTION

The retinal pigment epithelium (RPE) is a polarized monolayer of cells that forms a part of the blood–retina barrier in the back of the vertebrate eye. This epithelium separates the choroidal blood supply from the extracellular or subretinal space (SRS) that surrounds the retinal photoreceptors. By transporting ions and fluid from the SRS to the choroid (Hughes et al., 1998; Maminishkis et al., 2002), the RPE plays a critical role in maintaining the volume and chemical composition of the SRS. Large amounts of CO_2 and H_2O are deposited into the SRS due to the high metabolic activity of the photoreceptors (Wangsa-Wirawan and Linsenmeier, 2003). The high choroidal blood flow, ≈1,200 ml/min/100 g (Alm and Bill, 1987), provides a sink for the removal of these metabolites. Failure to remove CO_2 would result in acidosis detrimental to retinal function (Sillman et al., 1972; Meyertholen et al., 1986; Takahashi et al., 1993). In addition, abnormal accumulation of fluid in the SRS can cause retinal detachment and degeneration (Fisher et al., 2005).

The RPE expresses several different HCO_3 transport proteins at the apical and basolateral membranes as illustrated in Fig. 1 (Hughes et al., 1989; Kenyon et al., 1997). As in other epithelia, the activities of these transporters in human RPE can be facilitated by carbonic anhydrases (CAs) expressed in the cytosol (CA II), on the apical membrane (CA IV, CA IX, CA XII, and CA XIV), or on the basolateral membrane (CA IX) (Casey, 2006; Purkerson and Schwartz, 2007; Zhi, C.G., F.E. Wang, T. Banzon, S. Jalickee, R. Fariss, A. Maminishkis, and S.S. Miller. 2007. Membrane-Bound Carbonic Anhydrases in Human Fetal Retinal Pigment Epithelial Cells (hfRPE)). The removal of CO_2 from the SRS can be achieved by diffusion across the RPE or by conversion to HCO_3 using the catalytic activity of CAs for transmembrane transport via HCO_3 transporters, or both. CO_2 diffusion into the RPE drives CA-mediated formation of HCO_3 and protons that acidify the cell. Transporter-mediated HCO_3 entry mitigates this acidification and helps maintain pH homeostasis in the RPE (Kenyon et al., 1997) and in the SRS (Borgula et al., 1989).

Correspondence to Sheldon S. Miller: millers@nei.nih.gov

Abbreviations used in this paper: AQP1, aquaporin 1; CA, carbonic anhydrase; CPE, choroid plexus epithelium; CSF, cerebrospinal fluid; DIDS, 4,4′-diisothiocyanostilbene-2,2′-disulfonic acid; DZA, dorzolamide; E_{NBC}, reversal potential of NBC; hfRPE, human fetal retinal pigment epithelium; J_V, steady-state fluid absorption rate; pH_i, intracellular pH; RPE, retinal pigment epithelium; R_T, total tissue resistance; SRS, subretinal space; TEP, transepithelial potential.

The Rockefeller University Press $30.00
J. Gen. Physiol. Vol. 133 No. 6 603–622
www.jgp.org/cgi/doi/10.1085/jgp.200810169

The close physiological relationship between HCO_3 and fluid transport was demonstrated in frog RPE, where steady-state fluid absorption was reduced by ≈70% after the removal of HCO_3 from both bathing solutions (Hughes et al., 1984). In cultured human fetal RPE (hfRPE), dorzolamide (DZA; nonspecific CA inhibitor) decreases steady-state fluid absorption (Zhi, C.G., F.E. Wang, T. Banzon, S. Jalickee, R. Fariss, A. Maminishkis, and S.S. Miller. 2007. Membrane-Bound Carbonic Anhydrases in Human Fetal Retinal Pigment Epithelial Cells (hfRPE)), suggesting the involvement of CA-mediated HCO_3 transport in fluid transport. These in vitro results are in contrast to in vivo animal studies that suggest that acetazolamide (nonspecific CA inhibitor) enhances retinal adhesion and SRS fluid clearance (Kita and Marmor, 1992; Wolfensberger et al., 2000). In addition, clinical studies showed that some patients with macular edema respond to acetazolamide treatment by increasing SRS fluid clearance (Cox et al., 1988; Fishman et al., 1989), but the underlying physiological mechanisms remain to be determined.

In vivo studies of retinal metabolism indicate an increase in SRS CO_2 level after the transition from light to dark (Wangsa-Wirawan and Linsenmeier, 2003). The present in vitro study investigates how an increase in apical CO_2 level can alter the activities of apical and basolateral membrane ion transporters to drive solute-linked fluid from the SRS to the choroid. We show that the RPE basolateral membrane has a significantly lower CO_2 permeability than the apical membrane. Therefore, an increase in apical CO_2 would cause an accumulation of intracellular CO_2 that is subsequently converted into HCO_3 by the catalytic activity of CA II; this in turn stimulates HCO_3 efflux at the basolateral membrane. We also show that the increase in apical CO_2 affects several ion transporters at the apical and basolateral membranes that would lead to a net increase in Na, Cl, and HCO_3 absorption and active solute-linked fluid transport across the RPE. The transition from light to dark is accompanied by an increase in photoreceptor metabolism. In vivo, the RPE can respond to the increased metabolic load by increasing the clearance of CO_2/HCO_3 and fluid from the SRS. This would help protect and maintain the health and integrity of the retina–RPE complex by preventing acidosis in the SRS and an abnormal separation of retina and RPE.

MATERIALS AND METHODS

hfRPE and bovine RPE preparation, and hfRPE culture

The methods used to extract intact native hfRPE monolayers and grow hfRPE cultures have been described previously (Maminishkis et al., 2006). Bovine RPE choroid was excised from fresh bovine eyes as described previously (Kenyon et al., 1997). The research presented in this study was performed in accordance with the tenets of the Declaration of Helsinki and the National Institutes of Health (NIH) institutional review board.

Intracellular pH (pH_i) measurements

Cultured hfRPE monolayer grown on a porous polyester membrane transwell filter was incubated at room temperature and 5% CO_2 for 30 min in Ringer solution containing 8 μM BCECF-AM (Invitrogen) pH-sensitive dye, 0.1% DMSO, and 0.01% pluronic acid. After incubation with BCECF-AM, the tissue was incubated in control (5% CO_2) Ringer for another 30 min before mounting on a mesh (250 μM) in a modified Üssing chamber (exposed surface area of 7.1 mm^2). The Üssing chamber was mounted on the stage of an axiovert-200 microscope (Carl Zeiss, Inc.) equipped with a 20× plan-neofluar objective. The hfRPE was continuously perfused with Ringer solution (equilibrated with 5% CO_2 at 36.5°C) at a flow rate of 2 ml × min^{-1}. Excitation photons (440/480 nm) were generated by a xenon light source, and the specific wavelengths were selected with a monochromator (Polychrome IV; Photonics). The emission fluorescence signals were captured with a photomultiplier tube (Thorn EMI). pH_i calibrations were performed by perfusing high-K calibration solutions (at pH 6.8, 7.2, and 7.6) containing 20 μM nigericin into both solution baths. The average calibration parameters were used to linearly correlate fluorescence intensity to pH_i for all pH-imaging experiments. We estimated the rate of dye loss from the RPE by calculating the percentage rate of loss of intracellular BCECF (k_{440}) at intervals of 0.5 min with the following equation (Bevensee et al., 1995):

$$k_{440} = \frac{I_{440}^{t=n+0.5} - I_{440}^{t=n}}{\Delta t \times I_{440}^{t=n}} \times 100\,,$$

where $(I_{440}^{t=n+0.5} - I_{440}^{t=n})$ is the difference in BCECF fluorescence intensity between Δt = 0.5-min intervals. From 30 experiments, the average k_{440} was $-2.21 \pm 0.50\% \times min^{-1}$.

Intracellular Na measurements

Cultured hfRPE monolayers were incubated in control Ringer containing 22 μM SBFI-AM (Invitrogen), 0.18% DMSO, and 0.02% pluronic acid for 1 h at room temperature and 5% CO_2. After incubating with SBFI-AM, the hfRPE was mounted onto the modified Üssing chamber. Fluorescent signals corresponding to intracellular Na concentration ($[Na]_i$) were obtained by alternating the excitation wavelength between 340 and 380 nm. A three-point calibration was performed at the end of the experiment (Harootunian et al., 1989). In brief, high K^+ (85-mM) calibration solutions containing 0, 10, or 30 mM [Na] and 10 μM gramicidin were perfused simultaneously to both the apical and basal baths. The fluorescence ratio for each $[Na]_o$ was used to obtain a calibration curve for the experiment.

Transepithelial potential (TEP) and total tissue resistance (R_T) measurements

TEP was measured with a pair of calomel electrodes in series with Ringer solution agar (4% wt/vol) bridges placed in the apical and basal baths of the Üssing chamber. The electrophysiology of the RPE was described previously in detail (Hughes et al., 1998). All TEP recordings are moving averages of 3 s. The R_T was calculated from Ohm's law,

$$R_T = \frac{\Delta TEP \cdot Area}{Current},$$

where ΔTEP is the TEP deflection when a 3-μA *Current* was passed across the hfRPE monolayer (once every minute) with Ag/AgCl electrodes, and *Area* is the cross-sectional surface area of the RPE. All hfRPE culture preparations had an $R_T \geq 200\ \Omega \times cm^2$.

Estimating intrinsic buffering capacity

The intrinsic buffering capacity (β_i mM/pH units) of the hfRPE cells was determined by using a previously described method

(Weintraub and Machen, 1989) and was fitted to a third-order polynomial: $\beta_i = -93.4 pH_i^3 + 2150.4 pH_i^2 + 16483.6 pH_i + 42065.6$ for $pH_i < 7.35$, and for $7.35 \le pH_i \le 7.7$, $\beta_i = 9.06$. The total buffering capacity (β_{total}) was then calculated with the equation, $\beta_{total} = \beta_i + \beta_{HCO_3} = \beta_i + 2.3[HCO_3]_i$. $[HCO_3]_i$ was estimated from the Henderson-Hasselbalch equation with the assumption that intracellular CO_2 level is 5%. H^+ flux was determined by multiplying β_{total} by an estimate of the initial dpH_i/dt determined from the pH_i response.

Steady-state fluid transport measurements

hfRPE monolayers cultured on porous membrane were mounted in a modified Üssing chamber, and the rate of transepithelial water flow (steady-state fluid absorption rate [J_V]) was measured using a refined capacitance probe technique as described previously (Hughes et al., 1984; Maminishkis et al., 2006). The TEP and R_T of the hfRPE monolayer were measured by injecting bipolar currents via Ag/AgCl pellet electrodes that were connected to the solution baths with agar bridges (4% wt/vol). All fluid transport experiments were performed in a Steri-Cult CO_2 incubator (Thermo Fisher Scientific) at 37°C and 5% CO_2. After a 15–30-min incubation in control Ringer (5% CO_2), steady-state J_V, TEP, and R_T were reached and recorded. Next, the incubator CO_2 control was set to 13%, and both bathing solutions were completely replaced with 13% CO_2-equilibrated Ringer. After waiting another 15–30 min for J_V, TEP, and R_T to reach steady state, the values of these parameters were recorded.

Ringer solutions and chemicals

The ionic composition of the control Ringer solution was based on MEM solution (Sigma-Aldrich). Control CO_2/HCO_3-buffered solution (pH 7.51 with 5% CO_2, pH 7.09 with 13% CO_2, and pH 8.20 with 1% CO_2) contains (in mM): 143.7 Na^+, 126.1 Cl^-, 26.2 HCO_3^-, 5 K^+, 1 $H_2PO_4^-$, 0.5 Mg^{2+}, 1.8 Ca^{2+}, 2 taurine, and 5 glucose. Low Cl (1 mM) Ringer (pH 7.5 when equilibrated with 5% CO_2) was prepared by replacing all Cl^-salts with gluconate salts (except for $MgCl_2$). The high gluconate concentration (128.7 mM) in the low Cl Ringer requires consideration of the strong Ca^{2+}- and Mg^{2+}-chelating ability of gluconate. By using the stability constants of Ca and Mg gluconate (Furia, 1972), the estimated free [Ca^{2+}] and [Mg^{2+}] in the low Cl Ringer are 0.6 and 0.3 mM, respectively. As a test, the low Cl Ringer was supplemented with additional Ca^{2+} (to 5.7 mM) and Mg^{2+} (to 0.84 mM) to give free [Ca^{2+}] and [Mg^{2+}] of 1.8 and 0.5 mM, respectively. This adjustment did not significantly affect the low basal bath [Cl]-induced pH_i, TEP, and R_T responses. Low HCO_3 Ringer (2.62 mM HCO_3; pH 6.5 when equilibrated with 5% CO_2) was prepared by replacing 23.58 mM $NaHCO_3$ with equimolar Na gluconate. Ca^{2+}/Mg^{2+}-free Ringer was made by replacing all $CaCl_2$ and $MgCl_2$ with 4.6 mM NMDG-Cl. Sucrose was added to Ringer solutions to achieve osmolarity of 300 ± 5 mOsm. 0.5 mM probenecid was added to all Ringer solutions used in pH_i and Na imaging experiments to slow dye leakage from the hfRPE. In fluid transport experiments, hfRPE culture media (300 mOsm and without any additives) equilibrated in 1, 5, or 13% CO_2 was used. DZA hydrochloride was purchased from U.S. Pharmacopeia. 4,4′-diisothiocyanostilbene-2,2′-disulfonic acid (DIDS) and nigericin were purchased from EMD. All other chemicals were purchased from Sigma-Aldrich.

All values within this report are presented as means ± SD. Statistical significance was evaluated by using the Student's *t* test (paired, two tailed). A p-value of <0.05 is considered statistically significant.

RESULTS

Apical or basal CO_2-induced pH_i responses in hfRPE

Fig. 2 A shows that increasing CO_2 from 5 to 13% in the apical or basal baths acidified the hfRPE by ≈0.25 and ≈0.04, respectively. Data from 13 experiments show that 13% apical CO_2 decreased pH_i by 0.23 ± 0.03, from 7.37 ± 0.05 to 7.14 ± 0.06; in contrast, the 13% basal bath CO_2-induced acidification (ΔpH_i = 0.03 ± 0.01) was almost eightfold smaller. Similarly in Fig. 2 B, decreasing CO_2 from 5 to 1% in the apical or basal baths alkalinized the hfRPE by ≈0.35 and ≈0.03, respectively. In four experiments, 1% apical or basal bath CO_2 alkalinized the cell by 0.41 ± 0.05 and 0.03 ± 0.03, respectively. The CO_2-induced changes in TEP and R_T were relatively small and not significant statistically. In freshly isolated native hfRPE preparations, 13% apical CO_2 also caused significantly larger acidification (ΔpH_i = 0.29 ± 0.04) than 13% basal CO_2 (ΔpH_i = 0.03 ± 0.02; n = 4). This difference in the apical/basolateral CO_2-induced pH_i response is even more pronounced in bovine RPE choroid preparations. No pH_i response to 13% basal CO_2 was

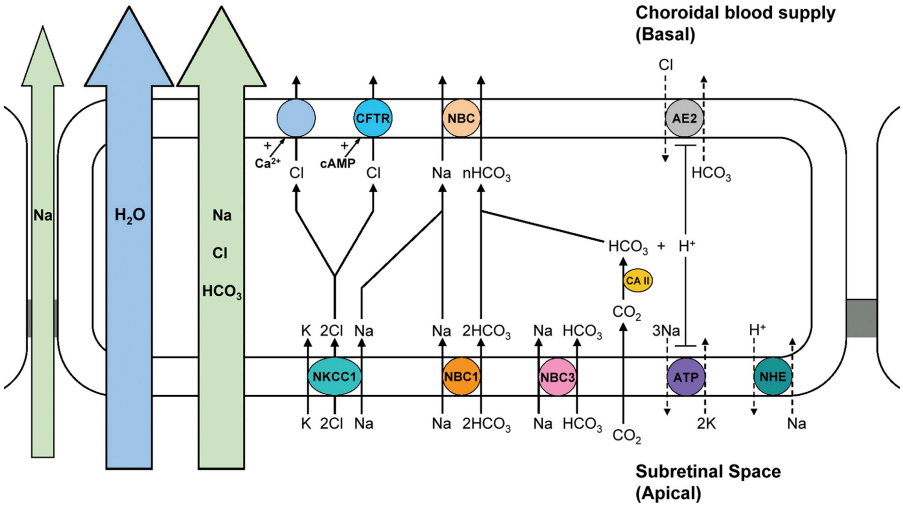

Figure 1. 13% apical CO_2 increases net solute and fluid absorption across the RPE. The transporters and channels depicted in this model are adopted from earlier studies of frog, bovine, human, and cultured human RPE. Apical membrane proteins: Na/K ATPase, Na/K/2Cl cotransporter (NKCC1), Na/H exchanger (NHE), and Na/$2HCO_3$ cotransporter (NBC1). Basolateral membrane proteins: Ca^{2+}-activated Cl channels, cAMP-sensitive CFTR, Cl/HCO_3 exchanger (AE2), and Na/$nHCO_3$ cotransporter (NBC). Increasing apical CO_2 increases Na (Cl + HCO_3) and fluid absorption from the SRS to the choroid.

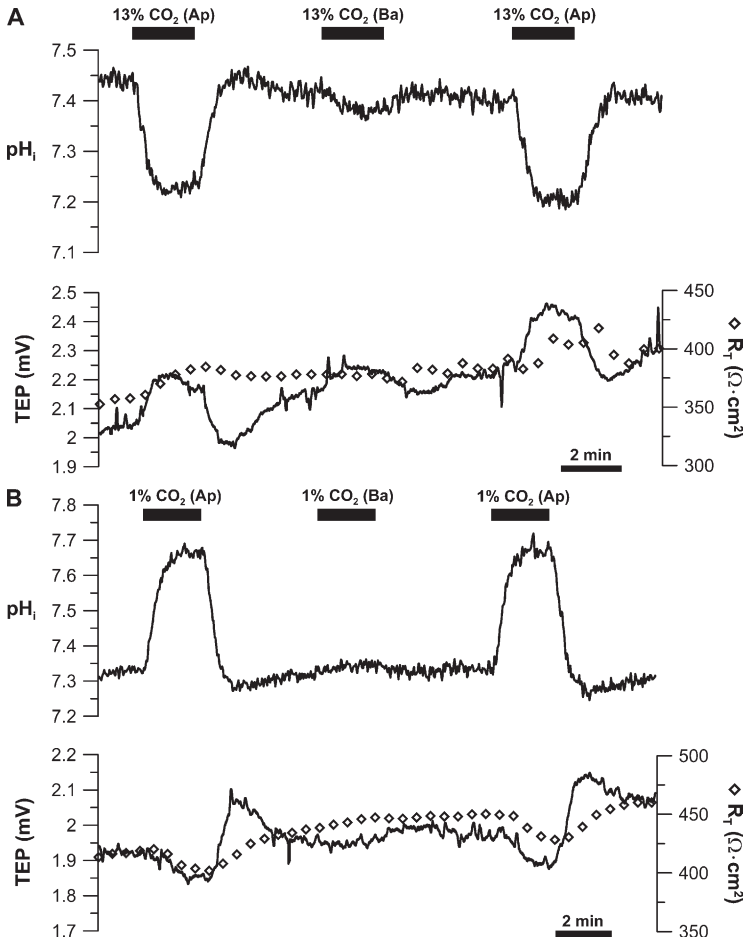

Figure 2. CO_2 flux across the apical and basolateral membranes. (A) 13% CO_2-equilibrated Ringer was perfused into the apical or basal bath. (B) 1% equilibrated Ringer was perfused into the apical or basal bath. The solid bars above the graph represent the beginning and end of a solution change (from control Ringer). The alteration in Ringer composition or the addition of drugs is indicated on the label above the solid bars. The time bar applies to pH_i, TEP, and R_T measurements and is located under the TEP/R_T panels. In each experiment, pH_i, TEP, and R_T were measured simultaneously.

observed, but a significant acidification was produced by 13% apical CO_2 ($\Delta pH_i = 0.39 \pm 0.09$; $n = 6$).

Tight junctions physically separate the RPE apical and basolateral membranes. Disruption of this barrier, by removing bath Ca^{2+} and Mg^{2+}, could provide a paracellular pathway for movement of CO_2 from the basal bath to the apical membrane. To test this notion, we increased basal bath CO_2 (from 5 to 13%) 15 min after the removal of Ca^{2+} and Mg^{2+} from both bathing solutions. Upon Ca^{2+} and Mg^{2+} removal, R_T rapidly decreased at a rate of $17.3 \pm 7.3\ \Omega \times cm^2 \times min^{-1}$ ($n = 5$). However, after 15 min in Ca^{2+}- and Mg^{2+}-free Ringer, the 13% basal bath CO_2-induced acidification was not significantly different than control (0.02 ± 0.01 vs. 0.02 ± 0.01; $n = 5$; $P > 0.05$), suggesting that basal bath CO_2 does not enter the apical membrane by diffusing across the tight junctions. When Ca^{2+} and Mg^{2+} were restored to the solution baths, R_T slowly recovered at a rate of $11.9 \pm 4.0\ \Omega \times cm^2 \times min^{-1}$, but the recovery rate decreases significantly after ≈15–20 min, and R_T recovered by only ≈40%.

Apical membrane electrogenic Na/2HCO_3 cotransporter in hfRPE

We tested apical Na/2HCO_3 cotransport activity by adding apical DIDS and comparing the resultant pH_i and TEP responses in control Ringer (26.2 mM HCO_3) versus low HCO_3 Ringer (2.62 mM HCO_3) in the apical bath (Fig. 3 A). Data from six experiments showed that in control Ringer, apical DIDS acidified the cell by 0.05 ± 0.02 and decreased TEP by 1.59 ± 0.63 mV, whereas adding apical DIDS in low apical bath [HCO_3] alkalinized the cell by 0.04 ± 0.01 and transiently increased TEP by 0.30 ± 0.15 mV; these responses are reversible. The apical DIDS-induced pH_i and TEP responses are consistent with the inhibition of an electrogenic HCO_3-dependent mechanism, whose activity can be reversed by a 10-fold reduction in apical bath [HCO_3].

To evaluate the potency of 0.5 mM of apical DIDS in the inhibition of the apical membrane Na/2HCO_3 cotransporter, we decreased apical bath [HCO_3] 10-fold and compared the resultant pH_i and TEP responses in the presence or absence of apical DIDS (Fig. 3 B). In three experiments, DIDS reduced the apical bath Δ[HCO_3]-induced TEP response by sevenfold, from 2.1 ± 0.2 to 0.3 ± 0.2 mV ($P < 0.01$). The effect of DIDS on the TEP response was partially reversible after a 5-min washout (ΔTEP = 1.28 ± 0.22 mV). This result suggests that apical DIDS almost completely blocked the apical membrane Na/2HCO_3 cotransporter activity. Surprisingly, the apical bath Δ[HCO_3]-induced acidification ($\Delta pH_i = 0.10 \pm 0.02$) was

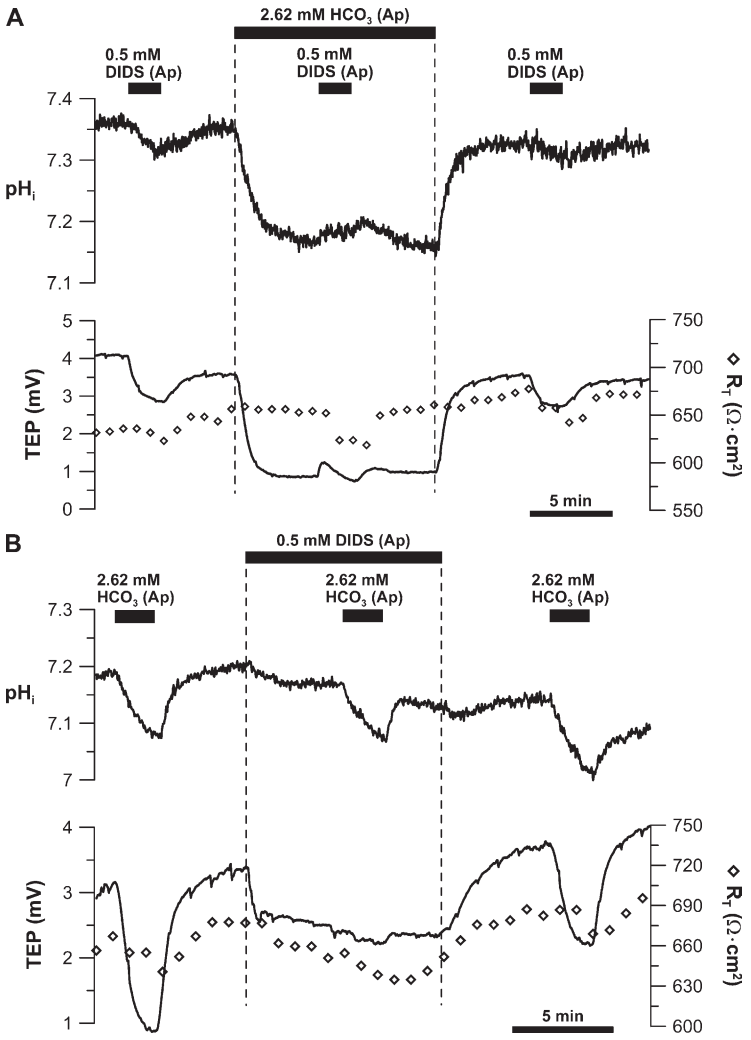

Figure 3. DIDS-sensitive $Na/2HCO_3$ cotransporter at the apical membrane. (A) 0.5 mM DIDS was added to the apical bath to obtain initial control response (pH_i, TEP, and R_T). The DIDS-induced response was then obtained in the presence of low (2.62 mM) HCO_3 Ringer in the apical bath. After washout with control Ringer, DIDS was added to the apical bath to obtain the final control response. (B) Low HCO_3 (2.62 mM) Ringer was perfused into the apical bath to obtain initial control response. The low basal bath [HCO_3]-induced response was then obtained in the presence of 0.5 mM of apical DIDS. After DIDS washout, low basal bath [HCO_3]-induced control response was obtained. Solid bars above the graphs represent solution changes from control Ringer as described in the legend to Fig. 2.

not significantly affected by DIDS ($\Delta pH_i = 0.09 \pm 0.01$; $n = 3$; $P > 0.05$), suggesting the presence of an electroneutral and DIDS-insensitive HCO_3 transporter at the apical membrane (see Discussion).

Apical bath CO_2 may be converted into HCO_3 by transmembrane CAs on the apical membrane surface, thus stimulating apical $Na/2HCO_3$ cotransport activity. Therefore, we tested the effect of altering apical bath CO_2 on apical $Na/2HCO_3$ cotransport activity by comparing apical DIDS (0.5 mM) -induced pH_i and TEP responses in control Ringer (5% CO_2) to that in 1 or 13% CO_2-equilibrated Ringer (Fig. 4 A). In four experiments, apical DIDS-induced pH_i and TEP responses in control Ringer ($\Delta pH_i = 0.05 \pm 0.02$; $\Delta TEP = 1.52 \pm 0.33$ mV) were the same as that in 13% CO_2-equilibrated Ringer ($\Delta pH_i = 0.05 \pm 0.02$; $\Delta TEP = 1.57 \pm 0.67$ mV; $P > 0.05$). Similarly, the apical DIDS-induced pH_i and TEP responses in control Ringer ($\Delta pH_i = 0.05 \pm 0.02$; $\Delta TEP = 1.66 \pm 0.59$ mV) were the same as that in 1% CO_2-equilibrated Ringer ($\Delta pH_i = 0.06 \pm 0.02$; $\Delta TEP = 1.31 \pm 0.78$ mV; $n = 5$; $P > 0.05$). To further test the pH_i sensitivity of the apical membrane $Na/2HCO_3$ cotransporter, we perfused 13% CO_2-equilibrated Ringer into the apical bath in the presence or absence of 0.5 mM of apical DIDS (Fig. 4 B). If increasing apical bath CO_2 increases apical $Na/2HCO_3$ cotransport activity, 13% apical CO_2 should cause a larger acidification in the presence of apical DIDS compared with control. However, in the presence of apical DIDS, the 13% CO_2-induced acidification ($\Delta pH_i = 0.22 \pm 0.03$) was the same as control ($\Delta pH_i = 0.22 \pm 0.02$; $n = 4$; $P > 0.05$). Collectively, these results lead to the conclusion that apical $Na/2HCO_3$ cotransport activity is not affected by apical CO_2-induced alterations in pH_i.

CA II catalyzes the interconversion of CO_2 and HCO_3 in the cytosol, and CA inhibition by DZA may affect apical $Na/2HCO_3$ cotransport activity. We tested this notion by decreasing apical bath [HCO_3] (10-fold) and compared the resultant pH_i and TEP responses in the presence of 250 μM of apical DZA to that in control (Fig. 5). In five experiments, DZA decreased apical bath Δ[HCO_3]-induced TEP response by 60% (from 2.25 ± 0.81 to 0.89 ± 0.29 mV; $P < 0.01$) and increased the pH_i response from 0.11 ± 0.01 to 0.19 ± 0.01 ($P < 0.01$). The effect of DZA on the pH_i and TEP responses was partially

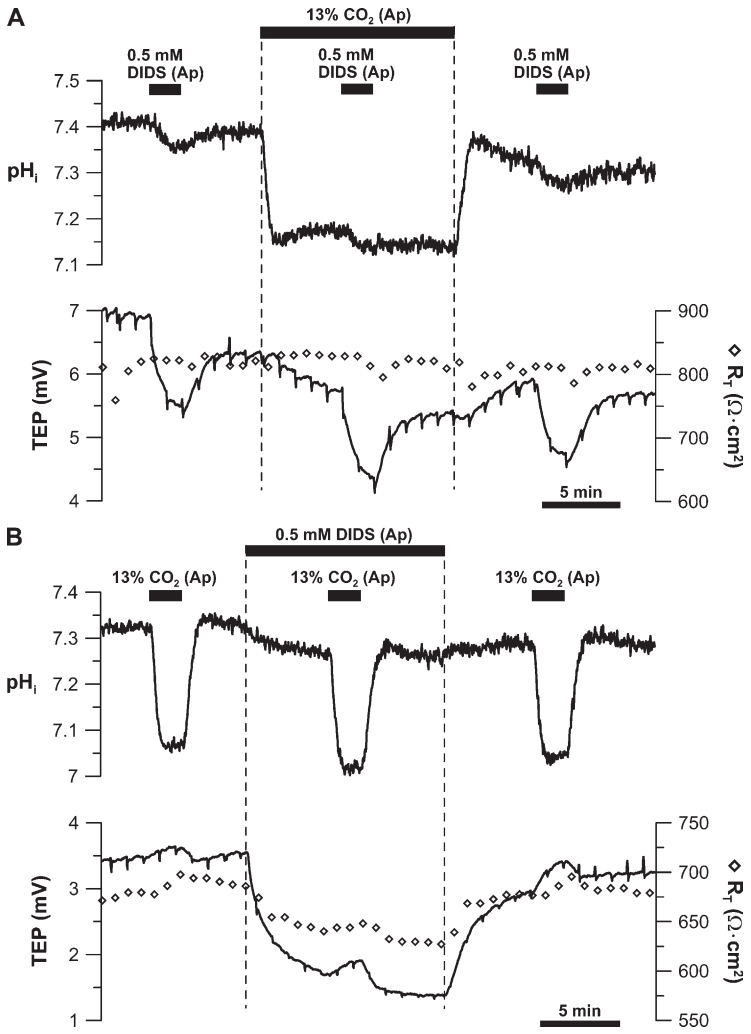

Figure 4. Effect of apical bath CO_2 on apical membrane $Na/2HCO_3$ cotransporter. (A) 0.5 mM DIDS was added to the apical bath to obtain initial control response. The DIDS-induced response was then obtained in the presence of 13% apical bath CO_2. After washout with control Ringer, DIDS was added to the apical bath to obtain the final control response. (B) 13% CO_2-equilibrated Ringer was perfused into the apical bath to record the initial control response. This maneuver was repeated in the presence of 0.5 mM of apical DIDS. After DIDS washout, 13% apical CO_2-induced control response was obtained. Solid bars above the graphs represent solution changes from control Ringer as described in the legend to Fig. 2.

reversible after a 5-min washout in control Ringer (ΔTEP = 1.27 ± 0.46 mV; ΔpH_i = 0.17 ± 0.02). The reduced apical bath $\Delta[HCO_3]$-induced TEP response in the presence of DZA indicates inhibition of apical $Na/2HCO_3$ cotransport activity. On the other hand, the apical bath $\Delta[HCO_3]$-induced acidification was larger in the presence of DZA because CA II inhibition reduces intracellular CO_2/HCO_3 buffering capacity, which compromises the ability of the RPE to buffer the acidification caused by HCO_3 efflux from the apical membrane.

Basolateral membrane Cl/HCO_3 exchanger activity in hfRPE

To assess basolateral membrane Cl/HCO_3 exchanger activity, basal bath [Cl] was reduced from 126 to 1 mM, which alkalinized the cell by ≈0.22 (Fig. 6). In three experiments, this alkalinization (ΔpH_i = 0.18 ± 0.05) was abolished by 0.5 mM of basal DIDS (ΔpH_i = 0.02 ± 0.01; n = 3; P < 0.05), but this effect was not reversible. Next, we tested the pH_i dependence of the Cl/HCO_3 exchanger by comparing the basal bath Δ[Cl]-induced pH_i response in 5 versus 13% apical bath CO_2 (Fig. 7 A). The steady-state pH_i in 5 and 13% apical bath CO_2 differed significantly, which required us to use the total buffering capacity of the hfRPE to calculate equivalent H^+ fluxes. In the presence of 13% CO_2-equilibrated Ringer in the apical bath, the basal bath Δ[Cl]-induced change in H^+ flux was 2.3 ± 1.0 mM × min^{-1}, approximately fourfold smaller than the H^+ flux in 5% CO_2 (9.0 ± 4.5 mM × min^{-1}; n = 7; P < 0.01); this effect was fully reversible. Fig. 7 B summarizes a parallel experiment in which basal bath [Cl] was reduced in the presence of 1% CO_2-equilibrated Ringer in the apical bath. In this case, the basal bath Δ[Cl]-induced proton flux was 27.4 ± 10.8 mM × min^{-1}, or approximately fivefold larger than the flux in 5% CO_2 (5.9 ± 6.5 mM × min^{-1}; n = 5; P = 0.01). These experiments indicate that the DIDS-sensitive basolateral membrane Cl/HCO_3 exchanger in hfRPE is pH_i dependent.

Basolateral membrane electrogenic $Na/nHCO_3$ cotransport in hfRPE

In confluent monolayers of hfRPE, reducing basal bath [HCO_3] 10-fold (5% CO_2) acidified the cells by 0.20 ± 0.05, with an equivalent H^+ flux of 6.2 ± 1.5 mM × min^{-1}

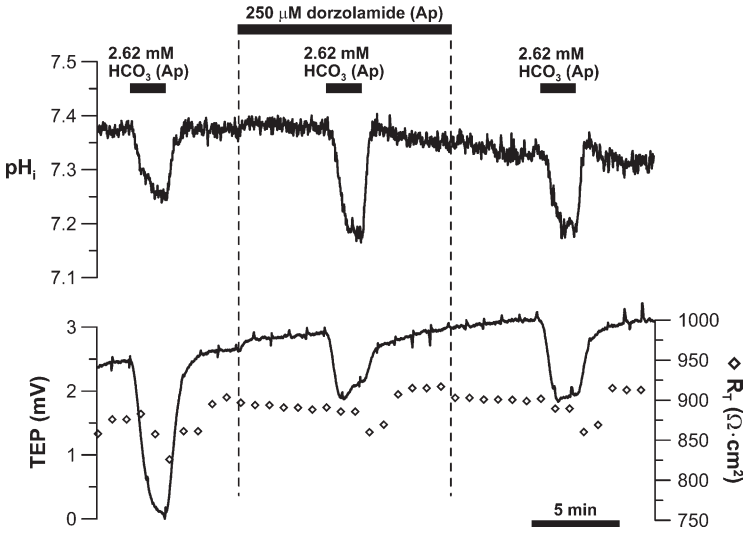

Figure 5. CA II dependence of apical membrane Na/$2HCO_3$ cotransporter. Low HCO_3 (2.62 mM) Ringer was perfused into the apical bath to record the initial control response. This maneuver was repeated in the presence of 250 μM of apical DZA. After DZA washout, low apical bath [HCO_3]-induced control response was obtained. Solid bars above the graphs represent solution changes from control Ringer as described in the legend to Fig. 2.

(n = 45), and increased TEP by 1.18 ± 0.60 mV (n = 53; Figs. 8–12 and Tables I and II). This TEP response is consistent with a basolateral membrane depolarization resulting from electrogenic Na/$nHCO_3$ cotransport activity. We evaluated the DIDS sensitivity of this basolateral membrane Na/$nHCO_3$ cotransporter by comparing the basal bath $\Delta[HCO_3]$-induced pH_i and TEP responses in the presence of 0.5 mM of basal DIDS to that in control (Fig. 8). In five experiments, basal DIDS reduced the basal bath $\Delta[HCO_3]$-induced acidification from 0.20 ± 0.04 to 0.09 ± 0.05 ($P < 0.05$), and reduced the TEP response from 1.41 ± 0.69 to 0.42 ± 0.29 mV ($P < 0.05$). The inhibitory effect of DIDS on the pH_i and TEP responses was irreversible after a 5-min washout with control Ringer (ΔpH_i = 0.12 ± 0.03; ΔTEP = 0.56 ± 0.25 mV; $P > 0.05$).

The Na dependence of the basolateral membrane HCO_3 transporter was studied by reducing basal bath [HCO_3] and measuring the resultant pH_i and TEP responses in the presence and absence of Na in both solution baths (Fig. 9). In three experiments, Na removal reduced the basal bath $\Delta[HCO_3]$-induced pH_i response by more than twofold (ΔpH_i = 0.08 ± 0.02) compared with control (ΔpH_i = 0.21 ± 0.04; $P < 0.05$). In addition, the basal bath $\Delta[HCO_3]$-induced TEP response (ΔTEP = 1.01 ± 0.21 mV) was essentially abolished in the absence of Na (ΔTEP = 0.04 ± 0.07 mV; $P < 0.05$), and this effect was reversible. This indicates that although reducing basal bath [HCO_3] causes HCO_3 efflux via both Cl/HCO_3 exchanger and Na/$nHCO_3$ cotransporter, the TEP response corresponds specifically to Na/$nHCO_3$ cotransporter activity due to its electrogenicity and Na dependence. This allows one to distinguish the activity of the Na/$nHCO_3$ cotransporter from that of the Cl/HCO_3 exchanger.

Basolateral Na/$nHCO_3$ cotransport: dependence on apical Na-linked transporters

We expected Na-linked transporters at the apical membrane (Fig. 1) to provide substrate that would help drive

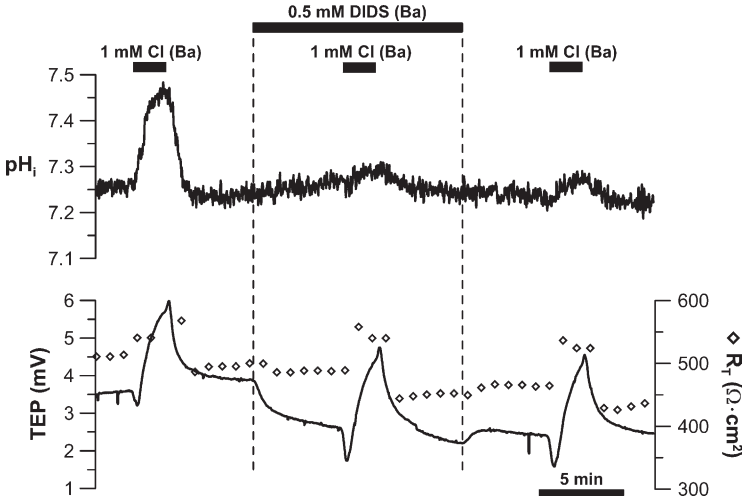

Figure 6. DIDS sensitivity of basolateral membrane Cl/HCO_3 exchanger. Low (1 mM) Cl Ringer was perfused into the apical bath to record the initial control response. This maneuver was repeated in the presence of 0.5 mM of apical DIDS. After DIDS washout, the low basal bath [Cl]-induced control response was obtained. Solid bars above the graphs represent solution changes from control Ringer as described in the legend to Fig. 2.

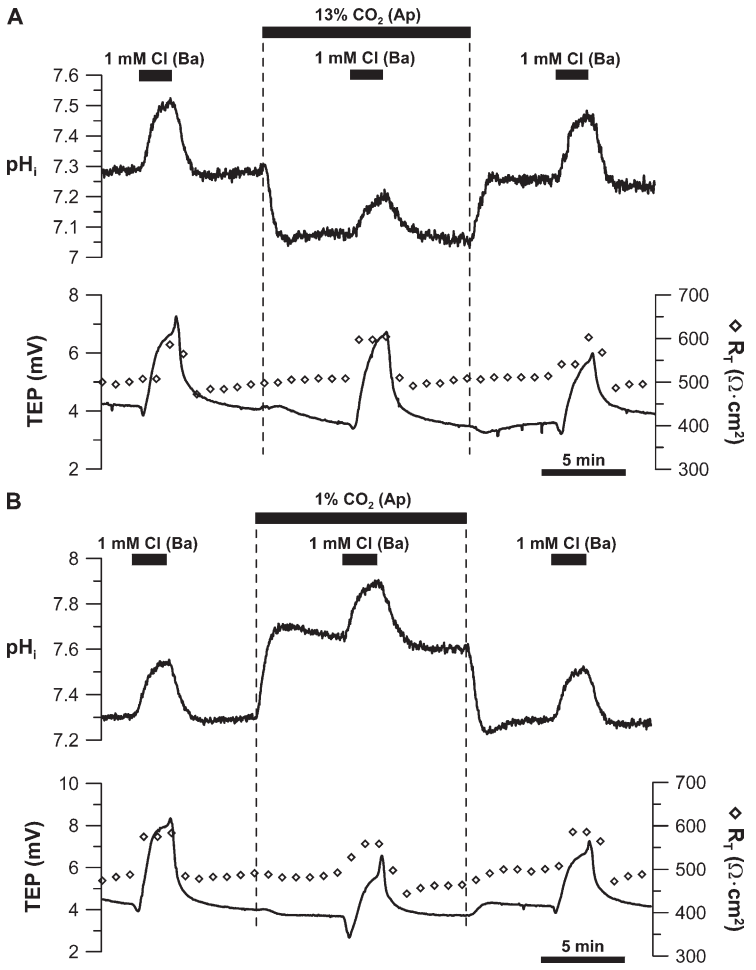

Figure 7. pH sensitivity of basolateral membrane Cl/HCO_3 exchanger. Low (1 mM) Cl Ringer was perfused into the apical bath to record the initial control response. This maneuver was then repeated in (A) 13% or (B) 1% apical bath CO_2. After returning to control Ringer, low basal bath [Cl]-induced control response was obtained. Solid bars above the graphs represent solution changes from control Ringer as described in the legend to Fig. 2.

the outward transport of $Na/nHCO_3$ at the basolateral membrane. To test this notion, we first inhibited the apical membrane Na/H exchanger with 1 mM amiloride and observed its effect on the pH_i and TEP responses caused by a 10-fold reduction in basal bath [HCO_3]. In five experiments, apical amiloride did not affect basal bath $\Delta[HCO_3]$-induced TEP response (ΔTEP = 1.28 ± 0.58 vs. 1.24 ± 0.50 mV; $P > 0.05$), indicating that the apical membrane Na/H exchanger does not provide substrate for basolateral $Na/nHCO_3$ cotransport activity. On the other hand, the basal bath $\Delta[HCO_3]$-induced acidification and H^+ flux was larger in the presence of apical amiloride (ΔpH_i = 0.28 ± 0.05; H^+ flux = 8.3 ± 1.6 mM × min^{-1}) compared with control (ΔpH_i = 0.22 ± 0.03; H^+ flux = 7.1 ± 1.3 mM × min^{-1}; $n = 5$; $P < 0.05$). This observation indicates that the Na/H exchanger normally acts to buffer cell acidification produced by HCO_3 efflux from the basolateral membrane.

Next, we inhibited the Na/K/2Cl cotransporter with 200 μM of apical bumetanide, which did not affect the basal bath $\Delta[HCO_3]$-induced pH_i response (ΔpH_i = 0.20 ± 0.03 vs. 0.21 ± 0.03 ; $n = 4$; $P > 0.05$) and TEP response (ΔTEP = 0.89 ± 0.28 vs. 0.80 ± 0.18 mV; $n = 6$; $P > 0.05$). This lack of effect suggests that Na entry via the Na/K/2Cl cotransporter does not contribute significantly to basolateral $Na/nHCO_3$ cotransport activity. We also evaluated the effect of Na extrusion by the apical membrane Na/K ATPase on the activity of the basolateral membrane $Na/nHCO_3$ cotransporter. Adding 200 μM ouabain into the apical bath caused an acute TEP decrease (ΔTEP = 0.55 ± 0.47 mV; $n = 5$), as expected from inhibition of the Na/K ATPase. However, apical ouabain did not affect the basal bath $\Delta[HCO_3]$-induced pH_i response (ΔpH_i = 0.18 ± 0.02 vs. 0.20 ± 0.02; $n = 3$; $P > 0.05$) and TEP response (ΔTEP = 1.26 ± 0.59 vs. 1.17 ± 0.49 mV; $n = 5$; $P > 0.05$), indicating that Na extrusion by the Na/K ATPase does not reduce or limit basolateral $Na/nHCO_3$ cotransport activity.

The basolateral membrane $Na/nHCO_3$ cotransporter may be dependent on Na and HCO_3 entry from the apical membrane via the electrogenic $Na/2HCO_3$ cotransporter, as shown in Fig. 1. We tested the coupling between the apical and basolateral membrane Na/HCO_3 cotransporters by decreasing basal bath [HCO_3] in the presence of 0.5 mM of apical DIDS (Fig. 10). In seven experiments, the basal bath $\Delta[HCO_3]$-induced TEP response decreased from 0.86 ± 0.17 to 0.49 ± 0.06 mV ($P < 0.05$) in the presence of apical DIDS,

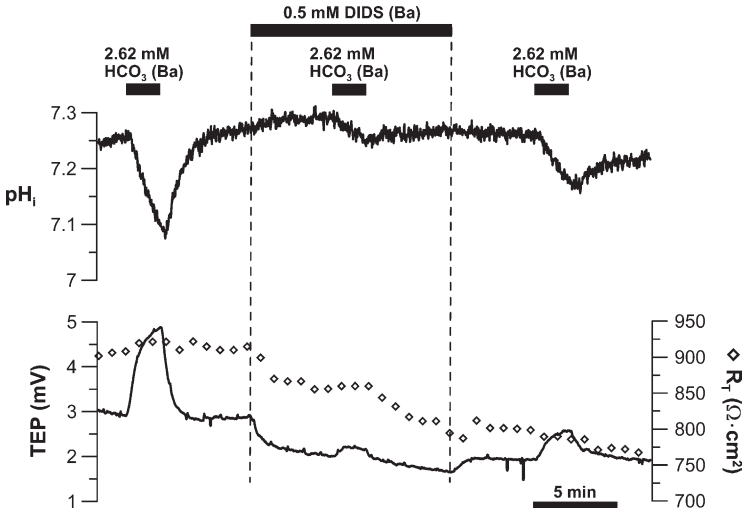

Figure 8. DIDS sensitivity of basolateral membrane $Na/nHCO_3$ cotransporter. Low HCO_3 (2.62 mM) Ringer was perfused into the basal bath to record the pH_i, TEP, and R_T responses, first in the absence and then in the presence of 0.5 mM of basal DIDS. After DIDS washout, low basal bath $[HCO_3]$-induced control response was obtained. Solid bars above the graphs represent solution changes from control Ringer as described in the legend to Fig. 2.

suggesting that inhibiting apical HCO_3 entry via the $Na/2HCO_3$ cotransporter reduces the HCO_3 supply that drives basolateral $Na/nHCO_3$ cotransport. However, apical DIDS increased the basal bath $\Delta[HCO_3]$-induced acidification from 0.19 ± 0.03 to 0.23 ± 0.03 ($P < 0.05$; $n = 7$), and H^+ flux from 5.0 ± 1.1 to 6.0 ± 1.1 mM × min^{-1} ($P < 0.05$; $n = 7$). This observation suggests that normally, apical HCO_3 entry via the $Na/2HCO_3$ cotransporter is a buffer that counteracts the acidification caused by HCO_3 efflux from the basolateral membrane.

Apical CO_2-induced changes in basolateral membrane $Na/nHCO_3$ cotransporter activity

Optimal $Na/nHCO_3$ cotransporter activity requires a steady supply of HCO_3, and the inhibition of CA II with DZA should reduce $Na/nHCO_3$ cotransport across the basolateral membrane. This notion was tested by reducing basal bath $[HCO_3]$ 10-fold in the presence of 250 μM DZA in the basal bath (Fig. 11). In a total of nine experiments, DZA reduced the basal bath $\Delta[HCO_3]$-induced TEP response by ≈30% (from ΔTEP = 1.44 ± 0.80 to 0.98 ± 0.50 mV; $P < 0.01$), suggesting that CA II inhibition reduces basolateral $Na/nHCO_3$ cotransport activity. In contrast, DZA did not affect the basal bath $\Delta[HCO_3]$-induced acidification (ΔpH_i = 0.18 ± 0.03) compared with control (ΔpH_i = 0.17 ± 0.01; $n = 4$; $P > 0.05$). This lack of effect probably occurred because the DZA-induced reduction in basolateral membrane HCO_3 efflux is counteracted by a concomitant reduction in intracellular CO_2/HCO_3 buffering capacity.

A 13% CO_2 load applied to the apical membrane should increase basolateral membrane $Na/nHCO_3$ cotransport activity by shifting intracellular CO_2/HCO_3 equilibrium toward the formation of HCO_3 (facilitated by CA II activity). To test this hypothesis, we made a 10-fold reduction in basal bath $[HCO_3]$ and compared the resultant pH_i and TEP responses in 5 versus 13% apical bath CO_2 (Fig. 12 A). With 13% apical bath CO_2, the basal bath $\Delta[HCO_3]$-induced TEP response (ΔTEP = 1.35 ± 0.78 mV) was ≈20% higher than control (ΔTEP = 1.11 ± 0.67 mV; $n = 9$; $P < 0.05$). However, there was no change in basal bath $\Delta[HCO_3]$-induced pH_i response in

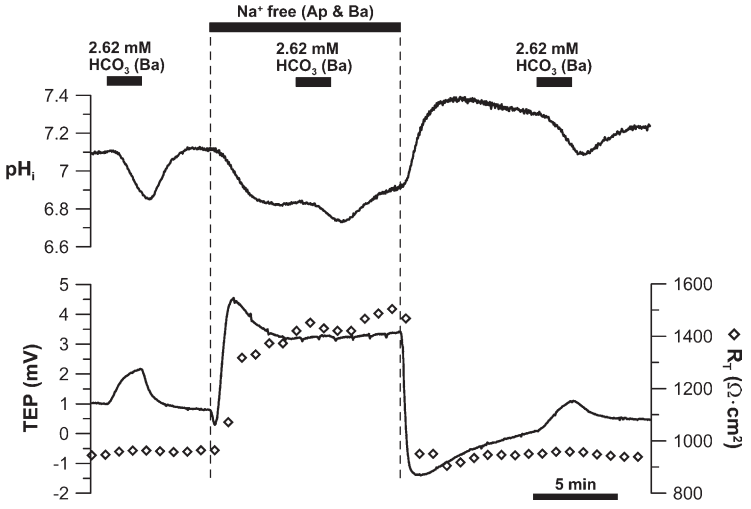

Figure 9. Na dependence of basolateral membrane $Na/nHCO_3$ cotransporter. Low HCO_3 (2.62 mM) Ringer was perfused into the basal bath to record the initial control response, and this maneuver was repeated in the absence of Na in both the apical and basal baths. After returning to control Ringer, low basal bath $[HCO_3]$-induced control response was obtained. Solid bars above the graphs represent solution changes from control Ringer as described in the legend to Fig. 2.

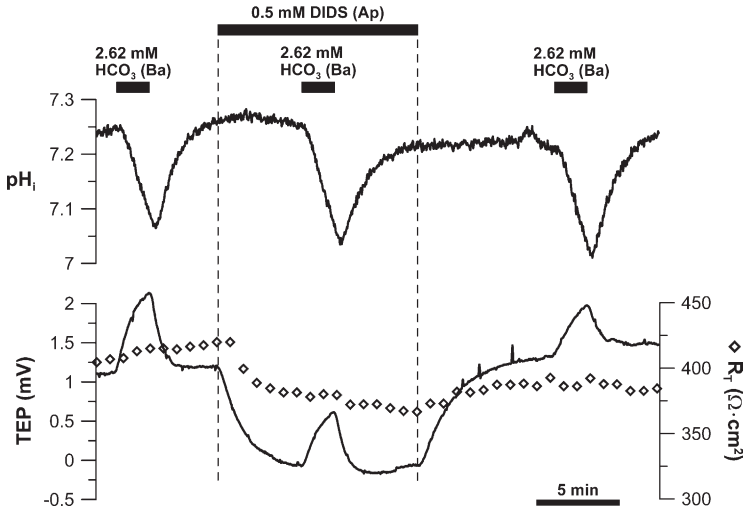

Figure 10. Linked activity of the apical and basolateral membrane Na/HCO_3 cotransporters. Low HCO_3 (2.62 mM) Ringer was perfused into the basal bath to obtain the initial control response, and this maneuver was then repeated in the presence of 0.5 mM of apical DIDS. After DIDS washout, the low basal bath $[HCO_3]$-induced control response was obtained. Solid bars above the graphs represent solution changes from control Ringer as described in the legend to Fig. 2.

the presence of 13% apical bath CO_2 (H^+ flux = 6.0 ± 1.3 mM × min^{-1}) compared with control (H^+ flux = 6.1 ± 2.3 mM × min^{-1}; n = 9; P > 0.05). Presumably, 13% apical CO_2 did not significantly alter H^+ flux caused by basal bath $\Delta[HCO_3]$ because the CO_2-induced increase in HCO_3 efflux via the $Na/nHCO_3$ cotransporter was offset by concomitant inhibition of the pH_i-sensitive Cl/HCO_3 exchanger, thus producing no observable change in net H^+ flux.

In similar experiments, we reduced basal bath $[HCO_3]$ in 1% apical bath CO_2 (Fig. 12 B). This maneuver should reduce free HCO_3 in the cell and subsequently decrease basolateral membrane $Na/nHCO_3$ cotransport activity. With 1% apical bath CO_2, the basal bath $\Delta[HCO_3]$-induced TEP response (ΔTEP = 0.37 ± 0.32 mV) was more than fivefold smaller than control (ΔTEP = 1.26 ± 0.74 mV; n = 5, P < 0.01). This result indicates that intracellular CO_2 is a significant source of HCO_3 supply for the basolateral membrane $Na/nHCO_3$ cotransporter. 1% apical CO_2 increased the basal bath $\Delta[HCO_3]$-induced equivalent H^+ flux from 7.2 ± 1.8 to 10.7 ± 1.9 mM × min^{-1} (n = 5; P = 0.04). The H^+ flux in the presence of 1% apical bath CO_2 was larger probably because the resultant alkalinization activated the Cl/HCO_3 exchanger more than the reduction in $Na/nHCO_3$ cotransport activity.

We showed that 13% apical CO_2 increased the basal bath $\Delta[HCO_3]$-induced TEP response (Fig. 12 A), suggesting that 13% apical CO_2 activates the basolateral membrane $Na/nHCO_3$ cotransporter, which should decrease $[Na]_i$. However, 13% apical CO_2 increased $[Na]_i$ from 15.7 ± 3.3 to 24.0 ± 5.3 mM (n = 6; P < 0.05). This suggests that one or more Na entry pathways are affected by 13% apical CO_2. To test whether 13% apical CO_2-induced acidification activated the Na/H exchanger, we compared the effect of 1 mM amiloride on the steady-state pH_i of the RPE in control Ringer (5% CO_2) to that in 13% CO_2-equilibrated Ringer. In three experiments, adding 1 mM amiloride into the apical bath did not cause any change in steady-state pH_i in 5 or 13% apical bath CO_2. As an additional test, we compared the magnitude of the 13% apical CO_2-induced

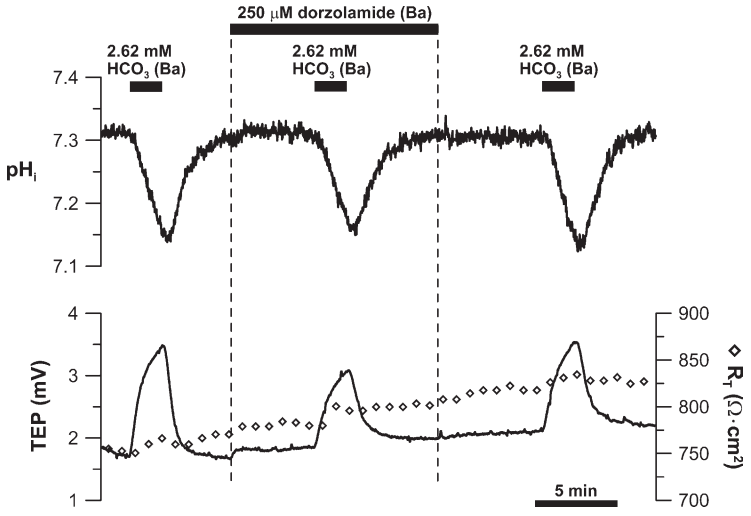

Figure 11. CA II dependence of basolateral membrane $Na/nHCO_3$ cotransporter. Low HCO_3 (2.62 mM) Ringer was perfused into the basal bath to record the pH_i, TEP, and R_T responses, first in the absence and then in the presence of 250 μM of basal DZA. After DZA washout, low basal bath $[HCO_3]$-induced control response was obtained. Solid bars above the graphs represent solution changes from control Ringer as described in the legend to Fig. 2.

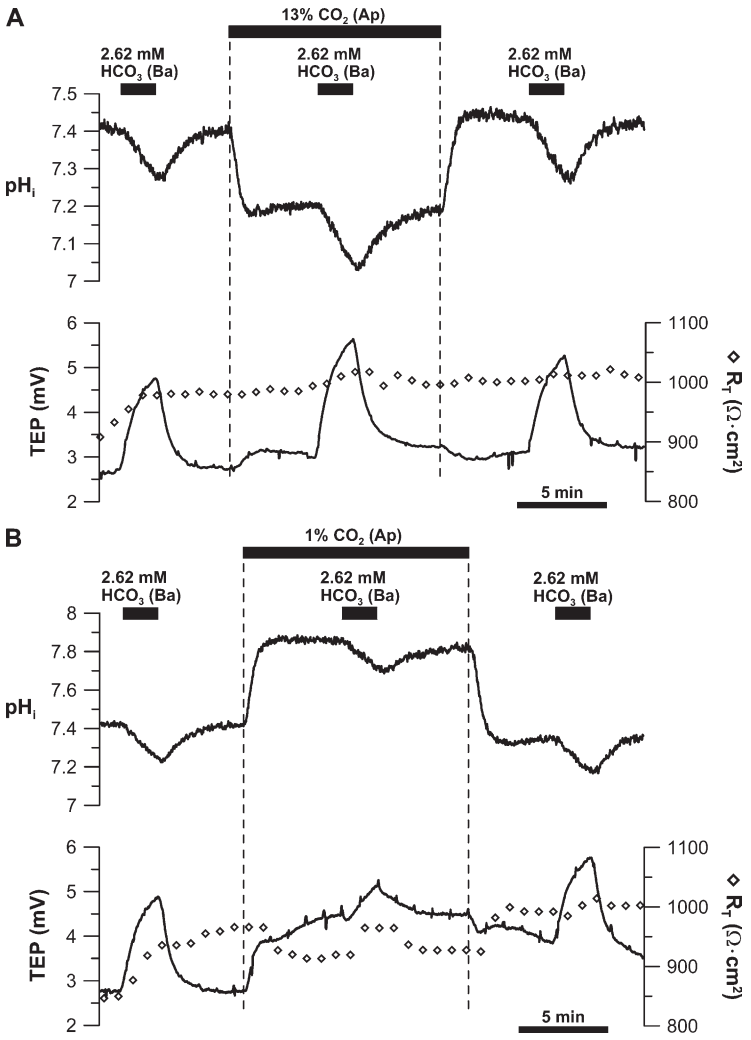

Figure 12. Effect of apical bath CO_2 on basolateral membrane Na/nHCO_3 cotransporter. Low HCO_3 (2.62 mM) Ringer was perfused into the basal bath to record the initial control response, and this maneuver was repeated in (A) 13% or (B) 1% apical bath CO_2. After returning to control Ringer, low basal bath [HCO_3]-induced control response was obtained. Solid bars above the graphs represent solution changes from control Ringer as described in the legend to Fig. 2.

acidification in the presence or absence of 1 mM amiloride in the apical bath. In four experiments, amiloride did not affect the 13% apical CO_2-induced acidification ($\Delta pH_i = 0.23 \pm 0.01$) compared with control ($\Delta pH_i = 0.22 \pm 0.02$; $P > 0.05$). These experiments indicate that 13% apical CO_2-induced acidification did not activate the Na/H exchanger.

CO_2- and HCO_3-mediated fluid absorption across RPE

We tested the role of the apical membrane Na/2HCO_3 cotransporter in fluid transport by adding 0.5 mM DIDS into the apical bath and measuring the resultant change in J_V. In four experiments, 0.5 mM of apical DIDS decreased J_V by more than twofold (from 16.7 ± 4.8 to 7.7 ± 3.7 µl × cm^{-2} × hr^{-1}; $P < 0.05$), suggesting that HCO_3 transport mediates a major component of fluid absorption across the RPE apical membrane. At the basolateral membrane, HCO_3 transporters and several Cl^- channels are DIDS sensitive. Not surprisingly, the addition of 0.5 mM DIDS to the basal bath decreased J_V from 20.3 ± 8.2 to 11.2 ± 6.0 µl × cm^{-2} × hr^{-1} ($n = 9$; $P < 0.05$).

The model in Fig. 1 predicts that 13% apical CO_2 would increase net Na, Cl, and HCO_3 absorption, producing an increase in J_V across the RPE. Fig. 13 A shows that 13% CO_2 increased J_V from ≈5 to 9 µl × cm^{-2} × hr^{-1}, and Fig. 13 B shows that 1% CO_2 decreased J_V from ≈7 to 2.5 µl × cm^{-2} × hr^{-1}. In four experiments, increasing CO_2 from 5 to 13% in both solution baths increased J_V by more than twofold (from 2.8 ± 1.6 to 6.7 ± 2.3 µl × cm^{-2} × hr^{-1}; $n = 5$; $P < 0.05$). In another set of experiments, decreasing CO_2 from 5 to 1% in both solution baths decreased steady-state fluid absorption by ≈60% (from 8.8 ± 3.9 to 3.4 ± 1.1 µl × cm^{-2} × hr^{-1}; $n = 4$; $P < 0.05$).

DISCUSSION

The retinal photoreceptors are among the most metabolically active cells in the body (Winkler et al., 2008). All of the oxygen used by the photoreceptors is supplied by the choroidal blood supply, as indicated by the steep decrease of PO_2 from ≈70 mm Hg in the choriocapillaris to ≈0 mm Hg at the photoreceptor cilium, which

TABLE I

Summary of basal bath Δ [HCO_3]-induced pH_i responses

Inhibitor/condition[a]		2.62 mM basal bath [HCO_3]-induced pH_i response[b]					
Apical	Basal	Data	Control	w/ inhibitor	Recovery	P[c]	*n*
	DIDS	ΔpH_i	−0.20 ± 0.04	−0.09 ± 0.05	−0.12 ± 0.03	<0.05	5
		H^+ flux	−6.5 ± 1.2	−3.6 ± 2.7	−4.3 ± 1.3	<0.05	
Na-free	Na-free	ΔpH_i	−0.21 ± 0.04	−0.08 ± 0.01	−0.14 ± 0.02	<0.05	3
		H^+ flux	−7.2 ± 1.7	−2.8 ± 0.7	−4.9 ± 0.8	<0.05	
amiloride		ΔpH_i	−0.22 ± 0.03	−0.28 ± 0.05	−0.21 ± 0.04	<0.05	5
		H^+ flux	−7.1 ± 1.3	−8.3 ± 1.6	−5.7 ± 1.4	<0.05	
bumetanide		ΔpH_i	−0.20 ± 0.03	−0.21 ± 0.03	−0.22 ± 0.03	>0.05	4
		H^+ flux	−6.9 ± 1.8	−6.8 ± 0.9	−7.6 ± 1.6	>0.05	
ouabain		ΔpH_i	−0.18 ± 0.02	−0.20 ± 0.02	−0.23 ± 0.03	>0.05	3
		H^+ flux	−5.1 ± 2.1	−5.4 ± 3.2	−5.7 ± 2.7	>0.05	
DIDS		ΔpH_i	−0.19 ± 0.03	−0.23 ± 0.03	−0.21 ± 0.01	<0.05	7
		H^+ flux	−5.0 ± 1.1	−6.0 ± 1.1	−5.3 ± 0.9	<0.05	
	DZA	ΔpH_i	−0.17 ± 0.01	−0.18 ± 0.03	−0.18 ± 0.02	>0.05	4
		H^+ flux	−5.2 ± 0.3	−5.1 ± 0.7	−5.6 ± 0.4	>0.05	
13% CO_2		ΔpH_i	−0.21 ± 0.05	−0.20 ± 0.03	−0.24 ± 0.04	>0.05	9
		H^+ flux	−6.0 ± 1.3	−6.1 ± 2.3	−6.5 ± 1.4	>0.05	
1% CO_2		ΔpH_i	−0.24 ± 0.08	−0.20 ± 0.06	−0.20 ± 0.06	>0.05	5
		H^+ flux	−7.2 ± 1.8	−10.7 ± 1.9	−6.0 ± 1.3	<0.05	

[a]Blank cells indicate that control Ringer was perfused into the corresponding bath.
[b]H^+ flux has units of mM × min^{-1}, and all values are reported as mean ± SD.
[c]The basal bath Δ[HCO_3]-induced pH_i response in control Ringer was compared to the pH_i response in the presence of the inhibitor/condition; $P < 0.05$ is considered significant by Student's *t* test.

forms the junction between inner and outer segments (Birol et al., 2007) and is the site of the most dense mitochondrial packing in the retina (Stone et al., 2008). Oxygen consumption at this location increases ≈1.5–3 times after dark adaptation, mainly from increased ATP consumption needed to maintain the photoreceptor dark current (Wangsa-Wirawan and Linsenmeier, 2003). The increase in retinal oxygen consumption leads to a proportionate increase in CO_2 production and its release into the SRS.

This CO_2 load would be mainly dissipated by the choroidal blood supply because it features a very high flow rate (Alm and Bill, 1987) and a relatively short diffusion path from the inner segments (Oyster, 1999). We perfuse 13% CO_2-equilibrated Ringer to the hfRPE apical membrane to mimic our estimate of the in vivo increase in CO_2 that occurs in the SRS after the transition from light to dark (from 5 to 10 ± 3%; see Appendix 1). The present results show that in hfRPE, CO_2 is more effectively transported across the apical membrane compared with the

TABLE II

Summary of basal bath Δ [HCO_3]-induced TEP responses

Inhibitor/condition[a]		2.62 mM basal bath [HCO_3]-induced TEP response (mV)[b]				
Apical	Basal	Control	w/ inhibitor	Recovery	P[c]	*n*
	DIDS	1.41 ± 0.69	0.42 ± 0.29	0.56 ± 0.25	<0.05	5
Na-free	Na-free	1.01 ± 0.21	0.04 ± 0.07	0.79 ± 0.38	<0.05	3
amiloride		1.28 ± 0.58	1.24 ± 0.50	1.23 ± 0.40	>0.05	5
bumetanide		0.89 ± 0.28	0.80 ± 0.18	0.97 ± 0.29	>0.05	6
ouabain		1.26 ± 0.59	1.17 ± 0.49	1.19 ± 0.51	>0.05	5
DIDS		0.86 ± 0.16	0.49 ± 0.07	0.63 ± 0.15	<0.05	6
	DZA	1.44 ± 0.80	0.98 ± 0.50	1.06 ± 0.55	<0.05	9
13% CO_2		1.11 ± 0.67	1.35 ± 0.78	1.07 ± 0.67	<0.05	9
1% CO_2		1.26 ± 0.74	0.37 ± 0.32	0.99 ± 0.59	<0.05	5

[a]Blank cells indicate that control Ringer was perfused into the corresponding bath.
[b]All values are reported as mean ± SD.
[c]The basal bath Δ[HCO_3]-induced TEP response in control Ringer was compared to the TEP response in the presence of the inhibitor/condition; $P < 0.05$ is considered significant by Student's *t* test.

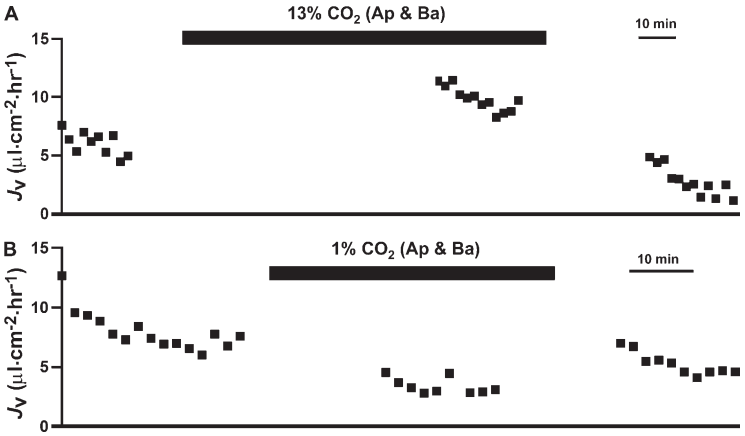

Figure 13. CO_2-induced changes in fluid absorption. 5% CO_2 equilibrated Ringer was added to both solution baths, and J_V was recorded with J_V, TEP, and R_T at steady state. The control Ringer was then replaced with either (A) 13% CO_2 or (B) 1% CO_2-equilibrated Ringer in both solution baths. J_V, TEP, and R_T values were recorded at steady state (15–30 min). Solid bars above the graphs represent solution changes from control Ringer as described in the legend to Fig. 2.

basolateral membrane probably because of a difference in exposed surface area (Miller and Steinberg, 1977; Maminishkis et al., 2006). Increasing apical bath CO_2 promotes CA II–dependent HCO_3 formation in the cytosol that can be transported across the basolateral membrane by a Na/nHCO_3 cotransporter. As previously shown in frog RPE, apical CO_2-induced acidification inhibits the basolateral membrane Cl/HCO_3 exchanger (Fig. 7 A), which can increase Cl recycling at the basolateral membrane, perhaps via CFTR or Ca^{2+}-activated Cl channels. The combination of this effect and the CO_2-induced increase in basolateral Na/nHCO_3 cotransport are hypothesized to increase net Na, Cl, and HCO_3 absorption, leading to the observed increase in steady-state fluid absorption across the RPE (Fig. 13).

Apical membrane CO_2 and HCO_3 transport

Earlier studies in frog and bovine RPE provide strong electrophysiological evidence for the electrogenic Na/$2HCO_3$ cotransporter at the apical membrane (Hughes et al., 1989; Kenyon et al., 1997). In addition, pNBC1 has been immunolocalized to the apical membrane of rat RPE (Bok et al., 2001). In hfRPE, we demonstrate apical Na/$2HCO_3$ cotransport activity with the following experimental observations: (1) Apical DIDS acidified the cell and decreased TEP, consistent with the inhibition of electrogenic Na/$2HCO_3$ cotransport into the cell. In addition, these DIDS-induced responses were reversed in the presence of low HCO_3 Ringer (10-fold) in the apical bath—apical DIDS alkalinized the cell and increased TEP. (2) Decreasing apical bath [HCO_3] decreased TEP, consistent with Na/$2HCO_3$ efflux across the apical membrane, and this response was essentially abolished by apical DIDS.

The presence of CA II and several apical membrane-bound CAs (e.g., CAs IV, IX, XII, and XIV) (Nagelhus et al., 2005) support the notion of HCO_3-mediated CO_2 transport from the SRS into the RPE via the electrogenic Na/$2HCO_3$ cotransporter. However, the following experiments suggest that increasing apical bath CO_2 does not stimulate apical Na/$2HCO_3$ cotransport: (1) apical DIDS caused pH_i and TEP responses in 5, 1, or 13% apical bath CO_2 that were statistically indistinguishable, and (2) the magnitude of 13% apical CO_2-induced acidification was unaffected by apical DIDS. This is probably because the fast CO_2/HCO_3 equilibration across the apical membrane prevented a change in the HCO_3 gradient. Besides NBC1 (SLC4A4; Gene ID 8671), a DIDS-insensitive and electroneutral Na/HCO_3 cotransporter, NBC3/NBCn1 (SLC4A7; Gene ID 9497) is also highly expressed at the apical membrane of human RPE (Wang, F.E., and S.S. Miller. 2007. Profiling MicroRNA (miRNA) Expression in Human Retina, Retinal Pigment Epithelium (RPE), and Choroid; Zhi, C.G., F.E. Wang, T. Banzon, S. Jalickee, R. Fariss, A. Maminishkis, and S.S. Miller. 2007. Membrane-Bound Carbonic Anhydrases in Human Fetal Retinal Pigment Epithelial Cells (hfRPE)). Our observation that apical DIDS had little effect on the apical bath $\Delta[HCO_3]$-induced acidification suggests that NBC3 is highly active in the RPE. However, this does not indicate that NBC1 has a lower activity than NBC3 because NBC1 is electrogenic and is therefore limited by both the membrane voltage and HCO_3 gradient. In contrast, NBC3 is limited only by the HCO_3 gradient. Thus, the relative activities of NBC1 and NBC3 cannot be accurately evaluated by comparing the apical bath $\Delta[HCO_3]$-induced pH_i responses in the presence versus absence of apical DIDS.

Apical membrane processes increase the effective apical surface area of native frog RPE by ≈30-fold relative to the basolateral surface area (Miller and Steinberg, 1977). Electron micrography of hfRPE provides evidence for similar structures in hfRPE (Maminishkis et al., 2006) and supports the notion of a relatively larger apical surface area. This difference suggests a possible basis for the approximately eightfold difference in the ΔpH_i produced by altering CO_2 (from 5 to 13%) in the apical versus basal bath, which allowed us to calculate a 10-fold difference between the relative CO_2 permeability of the apical and basolateral membranes of hfRPE cultures (see Appendix 1). However, in hfRPE cultures, CO_2 entry from the basal bath may be

hindered by the mesh support and transwell filter (attached to the basal membrane). The mesh was eliminated as a possible diffusion barrier by showing that the 13% basal bath CO_2 produced the same ΔpH_i with or without the mesh (unpublished data). To test the filter and its unstirred layer as a diffusion barrier, the hfRPE monolayer was uniformly damaged by mounting its apical membrane down on the mesh. This allows CO_2 from the basal bath to diffuse through the damaged areas and across the apical membrane of the RPE. If the filter was a significant barrier to CO_2, the difference between 13% apical and basal CO_2-induced ΔpH_i in a damaged hfRPE would be similar to that in an intact hfRPE (approximately eightfold). However, with the damaged hfRPE monolayer, the difference in CO_2-induced ΔpH_i was ≈2.5-fold ($n = 5$), and the calculated apparent relative CO_2 permeability was 3.0 ± 1.5, suggesting that the basolateral membrane is relatively less permeable to CO_2 than the apical membrane. Besides hfRPE cultures, significant differences between the 13% apical and basal bath induced pH_i responses were also observed in native bovine and fetal human RPE choroid preparations, thus corroborating our conclusion.

As another test of the basolateral membrane CO_2 permeability, basal bath CO_2 was increased from 5 to 13% in the absence of apical flow. In this case, the 13% basal CO_2-induced ΔpH_i was approximately threefold greater than with continuous apical perfusion ($n = 4$), suggesting that stopped apical flow increases the thickness of the unstirred layer at the apical membrane surface, which limits CO_2 diffusion out of the cell and causes a larger acidification. This result indicates that the basolateral membrane has some CO_2 permeability. Alternatively, the paracellular pathway may allow small amounts of CO_2 to enter the apical membrane from the basal bath. Tight junctions were disrupted by removing all Ca^{2+} and Mg^{2+} from both solution baths, but this maneuver did not increase the 13% basal CO_2-induced acidification; therefore, we conclude that the basolateral membrane is the main pathway for CO_2 entry from the basal bath.

A possible CO_2 transport mechanism arises from the ability of aquaporin 1 (AQP1) to function as a CO_2 channel (Cooper and Boron, 1998; Endeward et al., 2006). In cultured hfRPE cells, AQP1 mRNA is highly expressed in human RPE (Wang, F.E., and S.S. Miller. 2007. Profiling MicroRNA (miRNA) Expression in Human Retina, Retinal Pigment Epithelium (RPE), and Choroid). In addition, AQP1 was also detected exclusively at the apical membrane of hfRPE (unpublished data), corroborating an earlier study on rat RPE (Stamer et al., 2003). However, 1 mM pCMBS (nonspecific AQP1 inhibitor) did not block or inhibit CO_2 transport across the hfRPE apical membrane ($n = 3$), inconsistent with the AQP1 hypothesis. CO_2 barriers have been discovered at the apical membranes of gastric cells and colon epithelia (Waisbren et al., 1994; Endeward and Gros, 2005), and the RPE may possess a basolateral membrane with a unique lipid composition that limits CO_2 flux. The influence of lipid composition and properties on gas permeability has been studied in lipid bilayers (Hill et al., 1999; Hill and Zeidel, 2000), a possibility that remains to be evaluated in RPE.

Basolateral membrane HCO_3 transporters

The DIDS-sensitive Cl/HCO_3 exchanger at the basolateral membrane of hfRPE was inhibited or activated under acidic (13% apical CO_2) or basic (1% apical CO_2) conditions, respectively, as in frog RPE (Lin and Miller, 1994). From our Affymetrix data, AE2 (SLC4A2; Gene ID 6522) is the only AE isoform detected in cultured fetal human RPE and in native adult and fetal human RPE. Because AE2 is known to be pH sensitive (Kurschat et al., 2006; Stewart et al., 2007), it is possibly the isoform located at the basolateral membrane of hfRPE. Because this exchanger was inhibited by 13% apical CO_2, the RPE requires an alternate HCO_3 efflux pathway at the basolateral membrane to mediate transepithelial HCO_3 absorption. The following observations indicate the presence of an electrogenic $Na/nHCO_3$ cotransporter at the basolateral membrane: (1) reducing $[HCO_3]$ at the basal bath increased TEP, consistent with a depolarization of the basolateral membrane; (2) this TEP increase was significantly inhibited (≈70%) in the presence of basal DIDS; and (3) this TEP increase was completely abolished in the absence of Na in both bathing solutions.

Our Affymetrix data on human RPE (native adult and fetal RPE, and cultured fetal RPE) (Wang, F.E., and S.S. Miller. 2007. Profiling MicroRNA (miRNA) Expression in Human Retina, Retinal Pigment Epithelium (RPE), and Choroid) show high mRNA expression levels for NBC1 (SLC4A4; Gene ID 8671) and NBC4/NBCe2 (SLC4A5; Gene ID 57835), both of which are candidates for the identity of the basolateral membrane $Na/nHCO_3$ cotransporter in human RPE. Although this cotransporter's identity is unknown, both NBC1 and NBC4 have been shown to transport $Na:HCO_3$ with a stoichiometry of 1:2 (Gross et al., 2001; Virkki et al., 2002), suggesting inward Na/HCO_3 cotransport from the basolateral membrane. However, NBC4 transports $Na:HCO_3$ with a 1:3 stoichiometry at the apical membrane of the choroid plexus epithelium (CPE) (Millar and Brown, 2008). Because both the RPE and the CPE derive from the neural ectoderm and share many similarities in HCO_3 transport mechanisms (Brown et al., 2004; Praetorius, 2007), it is possible that the RPE expresses NBC4 at the basolateral membrane and transports $Na/nHCO_3$ with a 1:3 $Na:HCO_3$ stoichiometry. In addition, our calculation of the reversal potential of the $Na/nHCO_3$ cotransporter indicates that a 1:3 stoichiometry is required for $Na/nHCO_3$ transport out of the cell; this calculation is

based on our estimation of resting $[Na]_i$ and pH_i in control Ringer (see Appendix 2).

The basolateral membrane $Na/nHCO_3$ cotransporter is more dependent on HCO_3 than Na as a substrate, as supported by the following experiments: (1) Reducing basal bath $[HCO_3]$ 10-fold caused a TEP response that was reduced in the presence of apical DIDS, suggesting that inhibiting NBC1 reduced basolateral $Na/nHCO_3$ cotransport activity. (2) The basal bath $\Delta[HCO_3]$-induced TEP response was reduced in the presence of basal DZA, suggesting that CA inhibition reduces basolateral $Na/nHCO_3$ cotransport. DZA reduces HCO_3 transport in two ways. First, DZA slows CA-mediated hydration of CO_2 to HCO_3. Second, DZA inhibits the apical membrane $Na/2HCO_3$ cotransporter, as indicated by the reduction of apical bath $\Delta[HCO_3]$-induced TEP response in the presence of apical DZA. (3) The basal bath $\Delta[HCO_3]$-induced TEP response was increased in 13% apical bath CO_2 and decreased in 1% apical bath CO_2. This suggests that apical CO_2 entry and its subsequent conversion into HCO_3 is an important source of HCO_3 substrate for basolateral $Na/nHCO_3$ cotransport activity.

In addition to showing that the basolateral membrane $Na/nHCO_3$ cotransporter is dependent on apical HCO_3 supply, we also eliminated Na as a limiting substrate for basolateral $Na/nHCO_3$ cotransport by examining three Na transport proteins at the apical membrane of the RPE (Hughes et al., 1998): (1) bumetanide-sensitive Na/K/2Cl cotransporter, (2) amiloride-sensitive Na/H exchanger, and (3) ouabain-sensitive Na/K ATPase. In hfRPE, the presence of bumetanide, amiloride, or ouabain in the apical bath had no effect on the basal bath $\Delta[HCO_3]$-induced TEP responses, suggesting that these Na transport mechanisms are not linked to basolateral $Na/nHCO_3$ cotransport activity. Collectively, our data indicate that the basolateral membrane $Na/nHCO_3$ cotransporter is mainly driven by HCO_3 supplied by NBC1-mediated $Na/2HCO_3$ entry and CA II–mediated hydrolysis of CO_2 to HCO_3.

Apical Na entry pathways and CO_2/HCO_3-driven fluid transport

13% apical CO_2 increased basolateral $Na/nHCO_3$ cotransport, which should decrease $[Na]_i$. However, Na imaging experiments showed that 13% apical CO_2 increased $[Na]_i$, suggesting that Na enters the RPE via apical membrane Na transport processes. Although the Na/H exchanger can be activated by intracellular acidification (Aronson et al., 1982; Dunham et al., 2004), the following experiments show that 13% apical CO_2 does not activate the Na/H exchanger: (1) the magnitude of the 13% apical CO_2-induced acidification was unaffected in the presence of apical amiloride, and (2) adding 1 mM amiloride into the apical bath did not affect the steady-state pH_i in 5 or 13% apical bath CO_2. These observations indicate that the Na/H exchanger could not have contributed to the CO_2-induced $[Na]_i$ increase. This lack of participation might have occurred for three reasons: (1) the 13% CO_2-induced acidification was too small; (2) there was no change in the proton gradient across the Na/H exchanger; and (3) the 13% CO_2-equilibrated Ringer is acidic relative to control (pH 7.09 vs. 7.5), and the low extracellular pH may have inhibited the Na/H exchanger (Aronson et al., 1983). We ruled out the first possibility with a 10-mM NH_4 prepulse that caused only ≈0.1 decrease in pH_i ($n = 4$) but still showed the characteristic Na/H exchanger–mediated pH_i recovery; in comparison, 13% apical CO_2 acidified the cell by >0.2 pH units. In addition, we showed that reducing basal bath $[HCO_3]$ acidified the cell by only ≈0.2 but was able to activate the Na/H exchanger. $Na/2HCO_3$ entry via NBC1 was eliminated as a possible cause of the 13% apical CO_2-induced $[Na]_i$ increase because: (1) the apical DIDS-induced pH_i and TEP responses were the same in 5 or 13% apical bath CO_2, and (2) the magnitude of the 13% apical CO_2-induced pH_i response was unaltered in the presence of apical DIDS.

In alveolar epithelium, Na/K ATPase activity is reduced by CO_2-induced acidification (Briva et al., 2007), suggesting the possibility of a similar effect in RPE. In frog RPE, 13% CO_2-induced acidification activated the Na/K/2Cl cotransporter after inhibition of the basolateral membrane Cl/HCO_3 exchanger and the subsequent reduction in intracellular [Cl] (Edelman et al., 1994). Both the 13% apical CO_2-induced inhibition of the Na/K ATPase and activation of the Na/K/2Cl cotransporter can increase $[Na]_i$, thus providing Na entry pathway across the apical membrane that can mediate solute-driven fluid absorption. But these mechanisms remain to be evaluated.

In bovine RPE, net active Cl absorption is mediated by the Na/K/2Cl cotransporter at the apical membrane (Edelman et al., 1994) and by Ca^{2+}-activated and cAMP/PKA-dependent CFTR Cl channels at the basolateral membrane (Joseph and Miller, 1991; Bialek et al., 1995; Hughes et al., 1998). Evidence for the expression and basolateral membrane localization of CFTR in hfRPE has been presented (Blaug et al., 2003). The 13% apical CO_2-induced activation of the Na/K/2Cl cotransporter and inhibition of the Cl/HCO_3 exchanger would both increase net Cl absorption across the RPE.

HCO_3 transport also plays a significant role in RPE fluid transport. Steady-state fluid absorption was decreased by ≈50% after the addition of apical DIDS, indicating that the DIDS-sensitive NBC1 mediates HCO_3-driven fluid transport. The presence of NBC3 at the apical membrane suggests that it also contributes to HCO_3-mediated fluid transport. In addition, DZA or acetazolamide decreases steady-state fluid absorption across hfRPE in vitro (Zhi, C.G., F.E. Wang, T. Banzon, S. Jalickee, R. Fariss, A. Maminishkis, and S.S. Miller. 2007. Membrane-Bound Carbonic Anhydrases in

Human Fetal Retinal Pigment Epithelial Cells (hfRPE)). These observations are corroborated in the present experiments by the DZA-induced inhibition of NBC1 at the apical membrane and the $Na/nHCO_3$ cotransporter at the basolateral membrane. Interestingly, animal models and clinical studies showed that systemically administered acetazolamide increases fluid absorption across the RPE (Wolfensberger, 1999). It has been proposed that acetazolamide increases RPE fluid absorption in vivo by affecting membrane-bound CAs at the basolateral membrane, but there are no known membrane-bound CAs at the basolateral membrane of native RPE (Zhi, C.G., F.E. Wang, T. Banzon, S. Jalickee, R. Fariss, A. Maminishkis, and S.S. Miller. 2007. Membrane-Bound Carbonic Anhydrases in Human Fetal Retinal Pigment Epithelial Cells (hfRPE)). In addition, acetazolamide readily permeates RPE basolateral membrane, which would reduce fluid absorption by inhibiting cytosolic CA II, as observed in vitro. Further experiments involving interactions between the distal retina, choroid, and RPE are required to reconcile the difference in the effect of CA inhibitors on RPE fluid transport in vivo and in vitro.

HCO_3-mediated solute and fluid transport in the CPE

Both the RPE and the CPE develop from neural ectoderm; therefore, it is not surprising to find many similarities in the solute transport mechanisms of these two epithelia (Hughes et al., 1998; Brown et al., 2004; Praetorius, 2007). As demonstrated in this study, HCO_3 transport mediates net solute and fluid absorption in human RPE. This is supported by experiments where acetazolamide or DZA reduced steady-state fluid absorption by ≈50% in hfRPE cultures (Zhi, C.G., F.E. Wang, T. Banzon, S. Jalickee, R. Fariss, A. Maminishkis, and S.S. Miller. 2007. Membrane-Bound Carbonic Anhydrases in Human Fetal Retinal Pigment Epithelial Cells (hfRPE)). Similarly in the CPE, HCO_3 transport is an important mediator of cerebrospinal fluid (CSF) production (Saito and Wright, 1983, 1984); CSF secretion is inhibited by basal DIDS (Deng and Johanson, 1989). In addition, acetazolamide reduces CSF secretion by ≈40% (Vogh et al., 1987). Acetazolamide is used to prevent cerebral edema at high altitudes (Wright et al., 2008) and to reduce CSF pressure in children with hydrocephalus (Cowan and Whitelaw, 1991). The inhibitory effect of acetazolamide on CSF secretion led to the notion that CO_2 entry into the CPE from the blood plasma and the subsequent hydration of CO_2 into HCO_3 stimulates $NaHCO_3$ secretion across the apical membrane. This conclusion is supported by experiments in cat CPE, where ≈40% of Na secretion is attributed to CA II–mediated HCO_3 formation from CO_2 (Vogh and Maren, 1975). Perhaps not surprising, this mechanism of CO_2-driven HCO_3 transport is also found in the RPE.

Despite many similarities, the RPE normally absorbs Na (Cl + HCO_3) and fluid, whereas the CPE secretes Na (Cl + HCO_3) and fluid that helps form CSF. As in the RPE, the CPE expresses Na/HCO_3 cotransporters at both the apical and basolateral membranes. However, the most striking difference is that both NBC1/NBCe1 and NBC3/NBCn1 in the RPE are expressed at the apical membrane (Zhi, C.G., F.E. Wang, T. Banzon, S. Jalickee, R. Fariss, A. Maminishkis, and S.S. Miller. 2007. Membrane-Bound Carbonic Anhydrases in Human Fetal Retinal Pigment Epithelial Cells (hfRPE)), whereas in the CPE, these two transporters are expressed at the basolateral membrane (Brown et al., 2004; Praetorius, 2007). This difference suggests that NBC4, which is found at the apical membrane of the CPE (Millar and Brown, 2008), may be the unidentified $Na/nHCO_3$ cotransporter at the basolateral membrane of the RPE. We hypothesize that the difference in the membrane location of these HCO_3 transporters (i.e., NBC1, NBC3, and NBC4) in the RPE and CPE is the basis for their difference in HCO_3 and fluid transport direction.

If the CO_2-permeability difference of the apical and basolateral membranes of the RPE also manifests in the CPE, what is its functional significance? In the central nervous system, metabolic CO_2 produced by the brain is released into the CSF and subsequently neutralized by HCO_3 secreted from the CPE. We hypothesize that the CPE has a relatively lower CO_2 permeability at the apical membrane than at the basolateral membrane, and this property would promote CA II–mediated HCO_3 secretion across the apical membrane. This possibility remains to be evaluated.

Physiological implications

Upon dark adaptation, oxygen consumption in the retina increases (Kimble et al., 1980; Medrano and Fox, 1995; Cringle et al., 2002; Yu and Cringle, 2002), thus generating and depositing more CO_2 and H_2O into the SRS. Both CO_2 and H_2O generation can be estimated from the rate of oxygen consumption measured in situ in cat and nonhuman primate eyes (Wangsa-Wirawan and Linsenmeier, 2003). Our calculations (see Appendix 1) provide an estimate of CO_2 production in adult human photoreceptors of ≈0.29 and 0.54 mmol × hr^{-1} in light and dark, respectively. Considering that SRS [CO_2] is ≈2 mM, impaired CO_2 transport across the RPE could cause significant SRS or RPE acidification resulting in photoreceptor or RPE cell death. In addition, oxidative phosphorylation in the adult retina produces water at a rate of ≈0.5 µl × cm^{-2} × hr^{-1} in light and 0.9 µl × cm^{-2} × hr^{-1} in dark adapted eyes. Because glycolysis in the retina accounts for ≈95% of its total glucose consumption (Winkler et al., 2008), the combined retinal water production by aerobic respiration and glycolysis is calculated to be 3.6 and 6.5 µl × cm^{-2} × hr^{-1} in the light and dark, respectively. The CO_2-induced changes in ion

transport in the RPE is one of many events that follows the transition from light to dark in vivo. Others include: (1) an increase in SRS [K^+] from ≈3 to 5 mM, (2) the decrease in SRS [Ca^{2+}], and (3) the decrease in SRS pH (Steinberg et al., 1983; Borgula et al., 1989; Livsey et al., 1990; Yamamoto et al., 1992; Gallemore et al., 1994). Dark adaptation decreases SRS volume in situ (Li et al., 1994a,b). In addition, in a rat model of retinal reattachment (Maminishkis et al., 2002), fluid clearance from the SRS was faster in the dark-adapted eye (Maminishkis, A., personal communication), suggesting that steady-state fluid absorption across the RPE is higher in the dark.

In the dark-adapted eye, the high oxidative metabolism in the inner segments of the photoreceptors generates CO_2 and H_2O that are deposited into the SRS. The RPE uses the limited CO_2 diffusion at the basolateral membrane to drive Na, Cl, and HCO_3 transport across the RPE, which increases solute-driven fluid transport. This mechanism not only prevents CO_2 accumulation in the SRS, but it also removes water from the vicinity of the photoreceptors. This helps maintain the proper anatomical relationship between the photoreceptors and the RPE apical membrane, thus avoiding retinal detachment and photoreceptor degeneration (Stone et al., 1999; Wickham et al., 2006; Nakazawa et al., 2007).

APPENDIX 1

Relative CO_2 permeability

$$\frac{d[CO_2]}{dt} = D \cdot \left(CO_{2,in} - CO_{2,out}\right)$$

Differentiating the CO_2/HCO_3 equilibrium constant,

$$\frac{d[CO_2]}{dt} = \frac{[HCO_3^-]}{K_a} \cdot \frac{d[H^+]}{dt}$$

Combining the above equations gives

$$\frac{[HCO_3^-]_{in}}{K_a} \cdot \frac{d[H^+]_{Ap}}{dt} = D_{Ap} \cdot \left(CO_{2,in} - CO_{2,out}\right)$$

$$\frac{[HCO_3^-]_{in}}{K_a} \cdot \frac{d[H^+]_{Ba}}{dt} = D_{Ba} \cdot \left(CO_{2,in} - CO_{2,out}\right)$$

The relative permeability (P) of CO_2 at the apical versus the basolateral membrane is

$$P = \frac{D_{Apical}}{D_{Basal}} = \frac{d[H^+]_{Ap}}{dt} \div \frac{d[H^+]_{Ba}}{dt},$$

where D is the diffusion coefficient and $\frac{d[H^+]_{Ap}}{dt}$ and $\frac{d[H^+]_{Ba}}{dt}$ are the H^+ fluxes caused by perfusing 13% CO_2-equilibrated Ringer to the apical and basal bath, respectively. The H^+ fluxes were obtained by multiplying the 13% CO_2-induced dpH_i/dt with the total buffering capacity of the hfRPE. Based on these considerations, the relative permeability of apical versus basolateral membrane of hfRPE to CO_2 is 9.9 ± 4.4 (n = 7).

Retinal water production by aerobic respiration

In the dark, outer retina O_2 consumption (Wangsa-Wirawan and Linsenmeier, 2003) is 4.2 ± 0.5 ml O_2 × $100g^{-1}$ min^{-1}. In the light, outer retina O_2 consumption (Wangsa-Wirawan and Linsenmeier, 2003) is 2.3 ± 0.6 ml O_2 × $100g^{-1}$ min^{-1}. Wet weight of human retina (Bhosale and Bernstein, 2005) is 5.44 g. Oxygen consumption in the dark (density of oxygen at 36.9°C is 0.039 mmol/ml):

$$0.042\,ml\,O_2 \cdot g^{-1} min^{-1} \times 60\,min \cdot hr^{-1} \times$$
$$5.44\,g \times 0.0393\,mM \cdot ml^{-1} = 0.54\,mmol\,O_2 \cdot hr^{-1}$$

Oxygen consumption in the light:

$$0.023\,ml\,O_2 \cdot g^{-1} min^{-1} \times 60\,min \cdot hr^{-1} \times$$
$$5.44\,g \times 0.0393\,mM \cdot ml^{-1} = 0.29\,mmol\,O_2 \cdot hr^{-1}$$

In aerobic respiration, one molecule of water is generated for every molecule of oxygen consumed. Therefore, water generated in the dark is:

$$0.54\,mmol\,O_2 \cdot hr^{-1} \times 18\,mg \cdot mmol^{-1} \times$$
$$1\mu l \cdot mg^{-1} = 9.72\mu l\,H_2O \cdot hr^{-1}$$

Water generated in the light is:

$$0.29\,mmol\,H_2O \cdot hr^{-1} \times 18\,mg \cdot mmol^{-1} \times$$
$$1\mu l \cdot mg^{-1} = 5.22\mu l\,H_2O \cdot hr^{-1}$$

Assuming that the entire retina surface is 10.94 cm^2 (http://webvision.med.utah.edu/), the total rate of fluid generated by the retina through aerobic respiration in the dark is:

$$\frac{9.72\mu l\,H_2O / hr}{10.94\,cm^2} = 0.89\mu l\ H_2O \cdot cm^{-2} \cdot hr^{-1}$$

In the light:

$$\frac{5.31\mu l\,H_2O / hr}{10.94\,cm^2} = 0.48\mu l\ H_2O \cdot cm^{-2} \cdot hr^{-1}$$

Total retinal water production in the light and dark

For every glucose molecule that undergoes aerobic respiration, six molecules of CO_2 are produced. Therefore, glucose consumption by aerobic respiration in the dark is:

$$0.54\ mmol \cdot hr^{-1} \times \frac{1\,glucose}{6\,CO_2} = 0.09\,mmol \cdot hr^{-1}$$

Glucose consumption by aerobic respiration in the light is:

$$0.29\ mmol \cdot hr^{-1} \times \frac{1\,glucose}{6\,CO_2} = 0.05\,mmol \cdot hr^{-1}$$

Assuming that glycolysis in the retina accounts for 95% of glucose consumption in the dark (Winkler et al., 2008), the rate of water generation by glycolysis in the dark is:

$$0.09\,mmol \cdot hr^{-1} \times \frac{95}{5} \times \frac{2\,H_2O}{1\,glucose} \times \frac{18\,\mu l}{1\,mmol} \times \frac{1}{10.94\,cm^2} = 5.6\,\mu l \cdot cm^{-2} \cdot hr^{-1}$$

The rate of water generation by glycolysis in the light is:

$$0.05\,mmol \cdot hr^{-1} \times \frac{95}{5} \times \frac{2\,H_2O}{1\,glucose} \times \frac{18\,\mu l}{1\,mmol} \times \frac{1}{10.94\,cm^2} = 3.1\,\mu l \cdot cm^{-2} \cdot hr^{-1}$$

Total water produced by aerobic respiration and glycolysis in the dark is:

$$0.89 + 5.6 = 6.5\ \mu l \bullet cm^{-2} \bullet hr^{-1}$$

Total water produced by aerobic respiration and glycolysis in the light:

$$0.48 + 3.1 = 3.6\ \mu l \bullet cm^{-2} \bullet hr^{-1}$$

J_V of human RPE in vivo has been estimated using B-scan ultrasonography to be ≈11 $\mu l \times cm^{-2} \times hr^{-1}$ (Chihara and Nao-i, 1985), comparable to our in vitro measurements (Fig. 13).

CO_2 production in the light and dark

CO_2 production = O_2 consumption. CO_2 production in the dark is 4.2 ± 0.5 ml $CO_2 \times 100\ g^{-1}\ min^{-1}$, and in light is 2.3 ± 0.6 ml $O_2 \times 100\ g^{-1}\ min^{-1}$. Therefore, CO_2 production increases by 1.4–2.6-fold after transitioning from light to dark. This increase in CO_2 production translates to an increase in SRS CO_2 concentration, from 5 to 10 ± 3%.

APPENDIX 2

Na/nHCO_3 cotransporter reversal potential calculation

$$E_{NBC} = \frac{2.3RT}{F(n-1)} \log\left(\frac{[Na^+]_{in}}{[Na^+]_{out}}\right)\left(\frac{[HCO_3^-]_{in}}{[HCO_3^-]_{out}}\right)^n$$

$[Na^+]_{in}$ = 15.7 mM, $[Na^+]_{out}$ = 143.7 mM, $[HCO_3^-]_{in}$ = 27.9 mM, and $[HCO_3^-]_{out}$ = 26.2 mM. n is the stoichiometry of the Na/nHCO_3 cotransporter. We calculated the reversal potential of the Na/nHCO_3 cotransporter NBC (E_{NBC}) to be −55.7 mV for a Na:HCO_3 transport stoichiometry of 1:2. In this case, E_{NBC} is more hyperpolarized than the average basolateral membrane potential (V_B = −49.8 ± 3.7 mV) (Maminishkis et al., 2006), and the Na/2HCO_3 cotransporter transports Na and HCO_3 into the cell. To transport Na/nHCO_3 out of the cell against the strong inward Na gradient in control conditions, E_{NBC} must be more depolarized than V_B, and this condition is achieved for a Na:HCO_3 transport stoichiometry of 1:3, where E_{NBC} = −27.0 mV.

The authors thank Drs. Nancy Philp, Lawrence Rizzolo, Sarah Sohraby, Terry Machen, Bret Hughes, and Barry Winkler for reading early versions of the manuscript and providing critical feedback.

This work is supported by the NIH Intramural Research Program.

Edward N. Pugh Jr. served as editor.

Submitted: 24 November 2008
Accepted: 5 May 2009

REFERENCES

Alm, A., and A. Bill. 1987. Ocular circulation. *In* Adler's Physiology of the Eye. 8th ed. R.A. Moses and W.M. Hart, editors. Mosby, St. Louis, MO. 183–203.

Aronson, P.S., J. Nee, and M.A. Suhm. 1982. Modifier role of internal H+ in activating the Na+-H+ exchanger in renal microvillus membrane vesicles. *Nature.* 299:161–163.

Aronson, P.S., M.A. Suhm, and J. Nee. 1983. Interaction of external H+ with the Na+-H+ exchanger in renal microvillus membrane vesicles. *J. Biol. Chem.* 258:6767–6771.

Bevensee, M.O., C.J. Schwiening, and W.F. Boron. 1995. Use of BCECF and propidium iodide to assess membrane integrity of acutely isolated CA1 neurons from rat hippocampus. *J. Neurosci. Methods.* 58:61–75.

Bhosale, P., and P.S. Bernstein. 2005. Quantitative measurement of 3′-oxolutein from human retina by normal-phase high-performance liquid chromatography coupled to atmospheric pressure chemical ionization mass spectrometry. *Anal. Biochem.* 345:296–301.

Bialek, S., D.P. Joseph, and S.S. Miller. 1995. The delayed basolateral membrane hyperpolarization of the bovine retinal pigment epithelium: mechanism of generation. *J. Physiol.* 484:53–67.

Birol, G., S. Wang, E. Budzynski, N.D. Wangsa-Wirawan, and R.A. Linsenmeier. 2007. Oxygen distribution and consumption in the macaque retina. *Am. J. Physiol. Heart Circ. Physiol.* 293:H1696–H1704.

Blaug, S., R. Quinn, J. Quong, S. Jalickee, and S.S. Miller. 2003. Retinal pigment epithelial function: a role for CFTR? *Doc. Ophthalmol.* 106:43–50.

Bok, D., M.J. Schibler, A. Pushkin, P. Sassani, N. Abuladze, Z. Naser, and I. Kurtz. 2001. Immunolocalization of electrogenic sodium-bicarbonate cotransporters pNBC1 and kNBC1 in the rat eye. *Am. J. Physiol.* 281:F920–F935.

Borgula, G.A., C.J. Karwoski, and R.H. Steinberg. 1989. Light-evoked changes in extracellular pH in frog retina. *Vision Res.* 29:1069–1077.

Briva, A., I. Vadasz, E. Lecuona, L.C. Welch, J. Chen, L.A. Dada, H.E. Trejo, V. Dumasius, Z.S. Azzam, P.M. Myrianthefs, et al. 2007. High CO2 levels impair alveolar epithelial function independently of pH. *PLoS One.* 2:e1238.

Brown, P.D., S.L. Davies, T. Speake, and I.D. Millar. 2004. Molecular mechanisms of cerebrospinal fluid production. *Neuroscience.* 129:957–970.

Casey, J.R. 2006. Why bicarbonate? *Biochem. Cell Biol.* 84:930–939.

Chihara, E., and N. Nao-i. 1985. Resorption of subretinal fluid by transepithelial flow of the retinal pigment epithelium. *Albrecht Von Graefes Arch. Klin. Exp. Ophthalmol.* 223:202–204.

Cooper, G.J., and W.F. Boron. 1998. Effect of PCMBS on CO2 permeability of Xenopus oocytes expressing aquaporin 1 or its C189S mutant. *Am. J. Physiol.* 275:C1481–C1486.

Cowan, F., and A. Whitelaw. 1991. Acute effects of acetazolamide on cerebral blood flow velocity and pCO2 in the newborn infant. *Acta Paediatr. Scand.* 80:22–27.

Cox, S.N., E. Hay, and A.C. Bird. 1988. Treatment of chronic macular edema with acetazolamide. *Arch. Ophthalmol.* 106:1190–1195.

Cringle, S.J., D.Y. Yu, P.K. Yu, and E.N. Su. 2002. Intraretinal oxygen consumption in the rat in vivo. *Invest. Ophthalmol. Vis. Sci.* 43:1922–1927.

Deng, Q.S., and C.E. Johanson. 1989. Stilbenes inhibit exchange of chloride between blood, choroid plexus and cerebrospinal fluid. *Brain Res.* 501:183–187.

Dunham, P.B., S.J. Kelley, and P.J. Logue. 2004. Extracellular Na+ inhibits Na+/H+ exchange: cell shrinkage reduces the inhibition. *Am. J. Physiol. Cell Physiol.* 287:C336–C344.

Edelman, J.L., H. Lin, and S.S. Miller. 1994. Acidification stimulates chloride and fluid absorption across frog retinal pigment epithelium. *Am. J. Physiol.* 266:C946–C956.

Endeward, V., and G. Gros. 2005. Low carbon dioxide permeability of the apical epithelial membrane of guinea-pig colon. *J. Physiol.* 567:253–265.

Endeward, V., R. Musa-Aziz, G.J. Cooper, L.M. Chen, M.F. Pelletier, L.V. Virkki, C.T. Supuran, L.S. King, W.F. Boron, and G. Gros. 2006. Evidence that aquaporin 1 is a major pathway for CO2 transport across the human erythrocyte membrane. *FASEB J.* 20:1974–1981.

Fisher, S.K., G.P. Lewis, K.A. Linberg, and M.R. Verardo. 2005. Cellular remodeling in mammalian retina: results from studies of experimental retinal detachment. *Prog. Retin. Eye Res.* 24:395–431.

Fishman, G.A., L.D. Gilbert, R.G. Fiscella, A.E. Kimura, and L.M. Jampol. 1989. Acetazolamide for treatment of chronic macular edema in retinitis pigmentosa. *Arch. Ophthalmol.* 107:1445–1452.

Furia, T.E. 1972. Sequestrants in foods. *In* CRC Handbook of Food Additives. Vol. 1. T.E. Furia, editor. CRC Press, Boca Raton, FL. 276.

Gallemore, R.P., J.D. Li, V.I. Govardovskii, and R.H. Steinberg. 1994. Calcium gradients and light-evoked calcium changes outside rods in the intact cat retina. *Vis. Neurosci.* 11:753–761.

Gross, E., N. Abuladze, A. Pushkin, I. Kurtz, and C.U. Cotton. 2001. The stoichiometry of the electrogenic sodium bicarbonate cotransporter pNBC1 in mouse pancreatic duct cells is 2 HCO(3)(-):1 Na(+). *J. Physiol.* 531:375–382.

Harootunian, A.T., J.P. Kao, B.K. Eckert, and R.Y. Tsien. 1989. Fluorescence ratio imaging of cytosolic free Na+ in individual fibroblasts and lymphocytes. *J. Biol. Chem.* 264:19458–19467.

Hill, W.G., and M.L. Zeidel. 2000. Reconstituting the barrier properties of a water-tight epithelial membrane by design of leaflet-specific liposomes. *J. Biol. Chem.* 275:30176–30185.

Hill, W.G., R.L. Rivers, and M.L. Zeidel. 1999. Role of leaflet asymmetry in the permeability of model biological membranes to protons, solutes, and gases. *J. Gen. Physiol.* 114:405–414.

Hughes, B.A., S.S. Miller, and T.E. Machen. 1984. Effects of cyclic AMP on fluid absorption and ion transport across frog retinal pigment epithelium. Measurements in the open-circuit state. *J. Gen. Physiol.* 83:875–899.

Hughes, B.A., J.S. Adorante, S.S. Miller, and H. Lin. 1989. Apical electrogenic NaHCO3 cotransport. A mechanism for HCO3 absorption across the retinal pigment epithelium. *J. Gen. Physiol.* 94:125–150.

Hughes, B.A., R.P. Gallemore, and S.S. Miller. 1998. Transport mechanisms in the retinal pigment epithelium. *In* The Retinal Pigment Epithelium. M.F. Marmor and T.J. Wolfensberger, editors. Oxford University Press, New York. 103–134.

Joseph, D.P., and S.S. Miller. 1991. Apical and basal membrane ion transport mechanisms in bovine retinal pigment epithelium. *J. Physiol.* 435:439–463.

Kenyon, E., A. Maminishkis, D.P. Joseph, and S.S. Miller. 1997. Apical and basolateral membrane mechanisms that regulate pHi in bovine retinal pigment epithelium. *Am. J. Physiol.* 273:C456–C472.

Kimble, E.A., R.A. Svoboda, and S.E. Ostroy. 1980. Oxygen consumption and ATP changes of the vertebrate photoreceptor. *Exp. Eye Res.* 31:271–288.

Kita, M., and M.F. Marmor. 1992. Retinal adhesive force in living rabbit, cat, and monkey eyes. Normative data and enhancement by mannitol and acetazolamide. *Invest. Ophthalmol. Vis. Sci.* 33:1879–1882.

Kurschat, C.E., B.E. Shmukler, L. Jiang, S. Wilhelm, E.H. Kim, M.N. Chernova, R.K. Kinne, A.K. Stewart, and S.L. Alper. 2006. Alkaline-shifted pHo sensitivity of AE2c1-mediated anion exchange reveals novel regulatory determinants in the AE2 N-terminal cytoplasmic domain. *J. Biol. Chem.* 281:1885–1896.

Li, J.D., R.P. Gallemore, A. Dmitriev, and R.H. Steinberg. 1994a. Light-dependent hydration of the space surrounding photoreceptors in chick retina. *Invest. Ophthalmol. Vis. Sci.* 35:2700–2711.

Li, J.D., V.I. Govardovskii, and R.H. Steinberg. 1994b. Light-dependent hydration of the space surrounding photoreceptors in the cat retina. *Vis. Neurosci.* 11:743–752.

Lin, H., and S.S. Miller. 1994. pHi-dependent Cl-HCO3 exchange at the basolateral membrane of frog retinal pigment epithelium. *Am. J. Physiol.* 266:C935–C945.

Livsey, C.T., B. Huang, J. Xu, and C.J. Karwoski. 1990. Light-evoked changes in extracellular calcium concentration in frog retina. *Vision Res.* 30:853–861.

Maminishkis, A., S. Jalickee, S.A. Blaug, J. Rymer, B.R. Yerxa, W.M. Peterson, and S.S. Miller. 2002. The P2Y(2) receptor agonist INS37217 stimulates RPE fluid transport in vitro and retinal reattachment in rat. *Invest. Ophthalmol. Vis. Sci.* 43:3555–3566.

Maminishkis, A., S. Chen, S. Jalickee, T. Banzon, G. Shi, F.E. Wang, T. Ehalt, J.A. Hammer, and S.S. Miller. 2006. Confluent monolayers of cultured human fetal retinal pigment epithelium exhibit morphology and physiology of native tissue. *Invest. Ophthalmol. Vis. Sci.* 47:3612–3624.

Medrano, C.J., and D.A. Fox. 1995. Oxygen consumption in the rat outer and inner retina: light- and pharmacologically-induced inhibition. *Exp. Eye Res.* 61:273–284.

Meyertholen, E.P., M.J. Wilson, and S.E. Ostroy. 1986. The effects of hepes, bicarbonate and calcium on the cGMP content of vertebrate rod photoreceptors and the isolated electrophysiological effects of cGMP and calcium. *Vision Res.* 26:521–533.

Millar, I.D., and P.D. Brown. 2008. NBCe2 exhibits a 3 HCO3(-):1 Na+ stoichiometry in mouse choroid plexus epithelial cells. *Biochem. Biophys. Res. Commun.* 373:550–554.

Miller, S.S., and R.H. Steinberg. 1977. Passive ionic properties of frog retinal pigment epithelium. *J. Membr. Biol.* 36:337–372.

Nagelhus, E.A., T.M. Mathiisen, A.C. Bateman, F.M. Haug, O.P. Ottersen, J.H. Grubb, A. Waheed, and W.S. Sly. 2005. Carbonic anhydrase XIV is enriched in specific membrane domains of retinal pigment epithelium, Muller cells, and astrocytes. *Proc. Natl. Acad. Sci. USA.* 102:8030–8035.

Nakazawa, T., T. Hisatomi, C. Nakazawa, K. Noda, K. Maruyama, H. She, A. Matsubara, S. Miyahara, S. Nakao, Y. Yin, et al. 2007. Monocyte chemoattractant protein 1 mediates retinal detachment-induced photoreceptor apoptosis. *Proc. Natl. Acad. Sci. USA.* 104:2425–2430.

Oyster, C.W. 1999. The Human Eye: Structure and Function. Sinauer Associates, Inc., Sunderland, MA. 766 pp.

Praetorius, J. 2007. Water and solute secretion by the choroid plexus. *Pflugers Arch.* 454:1–18.

Purkerson, J.M., and G.J. Schwartz. 2007. The role of carbonic anhydrases in renal physiology. *Kidney Int.* 71:103–115.

Saito, Y., and E.M. Wright. 1983. Bicarbonate transport across the frog choroid plexus and its control by cyclic nucleotides. *J. Physiol.* 336:635–648.

Saito, Y., and E.M. Wright. 1984. Regulation of bicarbonate transport across the brush border membrane of the bull-frog choroid plexus. *J. Physiol.* 350:327–342.

Sillman, A.J., W.G. Owen, and H.R. Fernandez. 1972. The generation of the late receptor potential: an excitation-inhibition phenomenon. *Vision Res.* 12:1519–1531.

Stamer, W.D., D. Bok, J. Hu, G.J. Jaffe, and B.S. McKay. 2003. Aquaporin-1 channels in human retinal pigment epithelium: role in transepithelial water movement. *Invest. Ophthalmol. Vis. Sci.* 44:2803–2808.

Steinberg, R.H., R.A. Linsenmeier, and E.R. Griff. 1983. Three light-evoked responses of the retinal pigment epithelium. *Vision Res.* 23:1315–1323.

Stewart, A.K., C.E. Kurschat, and S.L. Alper. 2007. Role of nonconserved charged residues of the AE2 transmembrane domain in regulation of anion exchange by pH. *Pflugers Arch.* 454:373–384.

Stone, J., J. Maslim, K. Valter-Kocsi, K. Mervin, F. Bowers, Y. Chu, N. Barnett, J. Provis, G. Lewis, S.K. Fisher, et al. 1999. Mechanisms of photoreceptor death and survival in mammalian retina. *Prog. Retin. Eye Res.* 18:689–735.

Stone, J., D. van Driel, K. Valter, S. Rees, and J. Provis. 2008. The locations of mitochondria in mammalian photoreceptors: relation to retinal vasculature. *Brain Res.* 1189:58–69.

Takahashi, K., D.B. Dixon, and D.R. Copenhagen. 1993. Modulation of a sustained calcium current by intracellular pH in horizontal cells of fish retina. *J. Gen. Physiol.* 101:695–714.

Virkki, L.V., D.A. Wilson, R.D. Vaughan-Jones, and W.F. Boron. 2002. Functional characterization of human NBC4 as an electrogenic Na+-HCO cotransporter (NBCe2). *Am. J. Physiol.* 282:C1278–C1289.

Vogh, B.P., and T.H. Maren. 1975. Sodium, chloride, and bicarbonate movement from plasma to cerebrospinal fluid in cats. *Am. J. Physiol.* 228:673–683.

Vogh, B.P., D.R. Godman, and T.H. Maren. 1987. Effect of AlCl3 and other acids on cerebrospinal fluid production: a correction. *J. Pharmacol. Exp. Ther.* 243:35–39.

Waisbren, S.J., J.P. Geibel, I.M. Modlin, and W.F. Boron. 1994. Unusual permeability properties of gastric gland cells. *Nature.* 368:332–335.

Wangsa-Wirawan, N.D., and R.A. Linsenmeier. 2003. Retinal oxygen: fundamental and clinical aspects. *Arch. Ophthalmol.* 121:547–557.

Weintraub, W.H., and T.E. Machen. 1989. pH regulation in hepatoma cells: roles for Na-H exchange, Cl-HCO3 exchange, and Na-HCO3 cotransport. *Am. J. Physiol.* 257:G317–G327.

Wickham, L., C.S. Sethi, G.P. Lewis, S.K. Fisher, D.C. McLeod, and D.G. Charteris. 2006. Glial and neural response in short-term human retinal detachment. *Arch. Ophthalmol.* 124:1779–1782.

Winkler, B.S., C.A. Starnes, B.S. Twardy, D. Brault, and R.C. Taylor. 2008. Nuclear magnetic resonance and biochemical measurements of glucose utilization in the cone-dominant ground squirrel retina. *Invest. Ophthalmol. Vis. Sci.* 49:4613–4619.

Wolfensberger, T.J. 1999. The role of carbonic anhydrase inhibitors in the management of macular edema. *Doc. Ophthalmol.* 97:387–397.

Wolfensberger, T.J., R.K. Chiang, A. Takeuchi, and M.F. Marmor. 2000. Inhibition of membrane-bound carbonic anhydrase enhances subretinal fluid absorption and retinal adhesiveness. *Albrecht Von Graefes Arch. Klin. Exp. Ophthalmol.* 238:76–80.

Wright, A., S. Brearey, and C. Imray. 2008. High hopes at high altitudes: pharmacotherapy for acute mountain sickness and high-altitude cerebral and pulmonary oedema. *Expert Opin. Pharmacother.* 9:119–127.

Yamamoto, F., G.A. Borgula, and R.H. Steinberg. 1992. Effects of light and darkness on pH outside rod photoreceptors in the cat retina. *Exp. Eye Res.* 54:685–697.

Yu, D.Y., and S.J. Cringle. 2002. Outer retinal anoxia during dark adaptation is not a general property of mammalian retinas. *Comp. Biochem. Physiol.* 132:47–52.